Integrated Modelling of Canopy Photosynthesis, Fluorescence, and the Transfer of Energy, Mass and Momentum in the Soil-Plant-Atmosphere Continuum (STEMMUS-SCOPE v1.0.0)

Yunfei Wang[a, b, c, e], Yijian Zeng[c], Lianyu Yu[c], Peiqi Yang[c], Christiaan Van der Tol[c], Qiang Yu[e], Xiaoliang Lü[e], Huanjie Cai[a, b, ※], Zhongbo Su[c, d, ※]

[a] College of Water Resources and Architectural Engineering, Northwest Agriculture and Forestry University, Yangling, China
[b] Institute of Water Saving Agriculture in Arid Regions of China (IWSA), Northwest Agriculture and Forestry University, Yangling, China
[c] Faculty of Geo-Information Science and Earth Observation, University of Twente, Enschede, the Netherlands
[d] Key Laboratory of Subsurface Hydrology and Ecological Effect in Arid Region of Ministry of Education, School of Water and Environment, Chang'an University, Xi'an, China
[e] State Key Laboratory of Soil Erosion and Dryland Farming on the Loess Plateau, Institute of Water and Soil Conservation, Northwest Agriculture and Forestry University, Yangling, China

※ Correspondence: Huanjie Cai (huanjiec@yahoo.com); Zhongbo Su (z.su@utwente.nl)

Abstract. Root water uptake by plants is a vital process that influences terrestrial energy, water, and carbon exchanges. In the soil, vegetation, and atmosphere interfaces, root water uptake and solar radiation predominantly regulate the dynamics and health of vegetation growth, which can be remotely monitored by satellites, using the soil-plant relationship proxy – solar-induced chlorophyll fluorescence. However, most current canopy photosynthesis and fluorescence models do not account for root water uptake, which compromises their applications under water stressed conditions. To address this limitation, this study integrated photosynthesis, fluorescence emission, and transfer of energy, mass and momentum in the soil-plant-atmosphere continuum system, via a simplified one-dimensional root growth model and a resistance scheme linking soil, roots, leaves and atmosphere. The coupled model was evaluated with field measurements of maize and grass canopies. The results indicated that the simulation of land surface fluxes was significantly improved by the coupled model, especially when the canopy experienced moderate water stress. This finding highlights the importance of enhanced soil heat and moisture transfer, as well as dynamic root growth, on simulating ecosystem functioning.

Key words: SCOPE model; STEMMUS model; Soil-Plant-Atmosphere Continuum (SPAC) system; Root Water Uptake (RWU); Root system growth

1. Introduction

Root water uptake (RWU) by plants is a critical process controlling water and energy exchanges between the land surface and the atmosphere and as a result the plant growth. The representation of RWU is an essential component of eco-hydrological

models that simulate terrestrial water, energy and carbon fluxes (Seneviratne et al., 2010; Wang and Smith, 2004). However, most of these models consider the above-ground processes in much greater detail than below-ground processes, and therefore, they have limited ability to represent the dynamic response of plant water uptake to water stress. A particular mechanism of importance for plants to mitigate water stress is the compensatory root water uptake (CRWU) which refers to the process by which water uptake from sparsely rooted but well-watered parts of the root zone compensates for stress in other parts (Jarvis, 2011). The failure to account for compensatory water uptake and the associated hydraulic lift from deep subsoil (Caldwell et al., 1998; Espeleta et al., 2004; Amenu and Kumar, 2007; Fu et al. 2016) can lead to significant uncertainties in simulating the plant growth and corresponding eco-hydrological processes (Seneviratne et al., 2010).

Because the spatial (i.e., one dimensional vertical) pattern of RWU is determined by the spatial distribution of the root system, the knowledge of which is essential for predicting the spatial distribution of water contents and water fluxes in soils. The distribution of roots and their growth are in turn sensitive to various physical, chemical, and biological factors, as well as to soil hydraulic properties that influence the availability of water ~~and oxygen~~ for plants (Beaudoin et al., 2009). Many attempts have been made in the past to develop root growth models that account for the influence of various environmental factors such as temperature, aeration, soil water availability, and soil compaction. Existing root growth models ranged from complex, three-dimensional root architecture models (Bingham and Wu, 2011; Leitner et al., 2010; Wu et al., 2005) to much simpler root growth models that are implemented within more complex models such as EPIC (Williams et al., 1989) and DSSAT (Robertson et al., 1993). Most of these models reproduce the measured rooting depth very well, but the distribution of new growth root is based on empirical functions rather than biophysical processes (Camargo and Kemanian, 2016) (Table 1).

Modelling RWU requires representation of above and below ground processes, which can be realized considering the flow of water from soil through the plant to the atmosphere (i.e., Soil-Plant-Atmosphere Continuum, SPAC model) (Guo, 1992). The SPAC model represents a good compromise between simplicity (i.e., a small number of tuning parameters) and the ability to capture non-linear responses of RWU (and subsequently the ecosystem functioning) to drought events. Specifically, the SPAC model calculates the CRWU term using the gradient between leaf water potential and soil water potential of each soil layer. The most important parameters in the SPAC model include the leaf water potential, stomatal resistance, and the root resistance. Different from other macroscopic models using the root distribution function, the SPAC model needs explicitly the root length density at each soil layer to calculate the root resistance for each soil layer (Deng et al. 2017). The most practical method for obtaining the root length density is using a root growth model.

On other hand, remote sensing of solar-induced chlorophyll fluorescence (*SIF*) has been deployed to understand and monitor the ecosystem functioning under drought stress using models for vegetation photosynthesis and fluorescence (Zhang et al., 2020; Mohammed et al., 2019; Shan et al., 2019; Zhang et al., 2018). SCOPE (Soil Canopy Observation, Photochemistry, and Energy Fluxes) is such a model, simulating canopy reflectance and fluorescence spectra in the observation directions, as well as photosynthesis, and evapotranspiration as functions of leaf optical properties, canopy structure, and weather variables (Van

der Tol et al. 2009). SCOPE model provides a valuable means to study the link between remote sensing signals~~vegetation appearance~~ and ecosystem functioning, however, it does not consider the water budget in soil and vegetation. As such, there is no explicit parametrization of the effects of soil moisture variations on the photosynthetic or stomatal parameters. Consequently, soil moisture effects are only 'visible' in SCOPE model if the lack of soil moisture affects the optical or thermal remote sensing signals~~appearance of the vegetation~~ (i.e., during water stress period). The lack of such link between soil moisture availability and remote sensing signals~~vegetation appearance~~ compromises the capacity of SCOPE for simulating and predicting drought events on vegetation functioning.

The change of vegetation optical appearance as a result of soil moisture variations can only explain partially the soil moisture effect on ecosystem functioning (Bayat et al., 2018), which leads to considerably biased estimations of the gross primary productivity *(GPP*) and evapotranspiration (*ET)* in water limited conditions. This presents a challenge for using SCOPE to ecosystems in arid and semi-arid areas, where water availability is the primary limiting factor for vegetation functioning. This challenge becomes even more relevant considering that soil moisture deficit or "ecological drought" is expected to increase in both frequency and severity at nearly all ecosystems around the world (Zhou et al., 2013). Bayat et al. (2019) incorporated the SPAC model into SCOPE to address water stress conditions at a grassland site, but the coupled model neglected the dynamic root distribution at different soil layers and soil moisture serves only as a model input coming from measurements.

In this study, the modelling of above-ground photosynthesis, fluorescence emission, and energy fluxes in the vegetation layer by SCOPE will be fully coupled with a two-phase mass and heat transfer model - ~~the soil heat and mass transfer by the~~ STEMMUS model (Simultaneous Transfer of Energy, Mass and Momentum in Unsaturated Soil) (more detailed description of STEMMUS can be found in the *section of methodology and data*), by considering RWU based on a root growth model. The root growth model and the corresponding resistance scheme (from soil, through roots and leaves, to atmosphere) will be integrated for the dynamic modelling of water stress and root system, enabling the seamless modelling of soil-water-plant energy, water and carbon exchanges as well as *SIF*, and thus directly linking the vegetation dynamics (and its optical and thermal appearance) on-process-level to soil moisture variability. The next *section of methodology and data* describes the coupling scheme between SCOPE and STEMMUS models and the data was used to validate the coupled model, followed by the *section of results and discussion* which verifies the coupled STEMMUS-SCOPE model at a maize agroecosystem and a grassland ecosystem located in semi-arid regions and explores the dynamic responses of leaf water potential and root length density to water stress. The summary of this study and the further challenges are addressed in the *section of conclusions*.

Table 1. Comparison of LSMs and crop models in terms of sink term calculation of soil water balance.

	Model	Sink term calculation of soil water balance	Root water uptake process		
			Hydraulic redistribution (Richards and Caldwell, 1987)	Compensatory uptake (Jarvis, 2011)	Root distribution
LSMs	CLM5.0	Root length density of each soil layer and water stress is applied by the hydraulic conductance model (Lawrence et al. (2020)	Extreme case of CRWU	Following Darcy's Law for porous media flow equations	Empirical function depends on the plant functional type
	CLM4.5	Actual transpiration, root fraction of each soil layer and soil integral soil water availability (Fu et al., 2016)	The Ryel et al. (2002) function	Not considered	Empirical function
	CLM4.0	Actual transpiration, root fraction of each soil layer and soil integral soil water availability (Couvreur et al. 2012, Sulis et al., 2019)	HRWU scheme (RWU model based on hydraulic architecture)	HRWU scheme	Empirical function
	CLM3 & IBIS2	Actual transpiration, physical root distribution and the water availability in each layer (Zheng and Wang, 2007)	The Ryel et al. (2002) function	Dynamic root water uptake	Empirical function
	CoLM	Potential transpiration, root fraction in each layer and water stress factor (Zhu et al., 2017)	The Ryel et al. (2002) and the Amenu and Kumar (2007) function	Empirical approach with a compensatory factor	Empirical function
	JULES	Potential transpiration, root fraction of each soil layer and a weighted water stress in each layer (Eller et al., 2020)	Not considered	Not considered	Exponential distribution with depth
	Noah-MP	Based on the gradient in water potentials between root and soil, and root surface area (Niu et al., 2010)	Extreme case of CRWU	Following Darcy's law for porous media flow equations	Process-based 1D root surface area growth model
	CABLE	Based on the gradient in water potentials between the leaf, stem, and the weighted average of the soil (De Kauwe et al., 2020)	Extreme case of CRWU	Following Darcy's law for porous media flow equations	Empirical function
Crop Models	APSIM	Potential transpiration and water supply factor, but neglect root distribution (Keating et al., 2003)	Not considered	Not considered	Empirical function
	CropSyst	Difference in water potential between the soil and the leaf, and a total soil–root–shoot conductance (Stöckle et al., 2003)	Not considered	Considered by the leaf and soil water potential	Linear decrease in soils with No limitations to root exploration
	DSSAT	Water uptake per unit of root length is computed as an exponential function, and the actual RWU is the minimum of potential transpiration and the maximum capacity of root water uptake (Jones et al., 2003)	Not considered	Water uptake per unit of root length as a function of soil moisture	Using an empirical function
	EPIC	EPIC assumes that water is used preferentially from the top layers, and the potential water supply rate decreases exponentially downward (Williams et al.,2014)	Not considered	Not considered	Not considered
	SWAP	Based on the potential transpiration, root fraction and an empiric stress factor relationship (van Dam, 2000)	Not considered	Based on soil water potential	Function of relative rooting depth
	WOFOST	The simplest one, it calculates water uptake as a function of the rooting depth and the water available in that rooting depth without regard to the soil water distribution with depth (Supit et al., 1994)	Not considered	Not considered	Empirical function
	SPACSYS	According to empirical root length density distribution in a soil layer, potential transpiration and soil moisture (Wu et al., 2005)	Not considered	Not considered	1D (empirical function) or 3D root system (process based)
	STICS	Based on the potential transpiration, root fraction, and soil water distribution, but not process based (Beaudoin et al., 2009)	Not considered	Not considered	1D root length density profile

2. Methodology and Data

2.1. SCOPE and SCOPE_SM Models

SCOPE is a radiative transfer and energy balance model (Van der Tol et al. 2009). It simulates the transfer of optical, thermal, and fluorescent radiation in the vegetation canopy and computes *ET* by using an energy balance routine. SCOPE includes a radiative transfer module for incident solar and sky radiation to calculate the top of canopy outgoing radiation spectrum, net radiation and absorbed photosynthetically active radiation (*aPAR*), a radiative transfer module for thermal radiation emitted by soil and vegetation to calculate the top of canopy outgoing thermal radiation and net radiation, an energy balance module for latent heat, sensible heat and soil heat flux, and a radiative module for chlorophyll fluorescence to calculate the top of canopy ~~radiance spectrum of fluorescence~~*SIF* (the observation zenith angle was set as zero degree in this study).

Compared to other radiative transfer models which simplify the radiative transfer processes based on Beer's law, SCOPE has well-developed radiative transfer modules which consider the various leaf orientation and multiple scattering. SCOPE can provide detailed information about net radiation of every leaf within the canopy. Furthermore, SCOPE incorporates an energy balance model which predicts not only the temperature of leaf but also the temperature of soil surface temperature (i.e., a vital boundary condition needed by STEMMUS). In the original SCOPE, soil is treated in a very simple way with several empirical functions describing the ground heat storage. Later, Bayat et al. (2019) extended the SCOPE model by including the moisture effects on the vegetation canopy, which results in the SCOPE_SM model. This model takes soil moisture as input and predicts the effects on several processes of vegetation canopy by using the SPAC concept. Appendix A.1 lists the main equations of calculating water stress factor within SCOPE (Bayat et al. 2019), and the detailed formulation of SCOPE is referred to Van der Tol et al. (2009).

SCOPE_SM provides the basic framework to couple SCOPE with a soil process model. However, both SCOPE and SCOPE_SM ignored the soil heat and mass transfer processes and the dynamics of root growth. This can be overcome by introducing the STEMMUS model.

2.2. STEMMUS Model

STEMMUS model is a two-phase mass and heat transfer model with explicit consideration of the coupled liquid, vapor, dry air and heat transfer in unsaturated soil (Zeng et al. 2011a,b; Zeng and Su, 2013; Yu et al. 2018). STEMMUS provides a comprehensive description of water and heat transfer in the unsaturated soil, which can compensate what is currently neglected in SCOPE. In STEMMUS, the soil layers can be set flexible which was better than previous SPAC model only considered the whole root zone soil water content as fixed layers (Williams et al., 1996). The water and heat transfer processes are vital for vegetation phenology development as well as freeze-thaw processes. The boundary condition needed by STEMMUS includes surface soil temperature, which is the output of SCOPE. In addition, STEMMUS already contained an empirical equation to

calculate root water uptake and a simplified root growth module to calculate root fraction profile. As such, STEMMUS has an ideal model structure to be coupled with SCOPE. The main governing equations of STEMMUS are listed in Appendix A.2.

2.3 Dynamic Root Growth and Root Water Uptake

To obtain the root resistance of each soil layer, we incorporated a root growth module to simulate the root length density profile (see Appendix A.3). The simulation of root growth refers to the root growth module in the INRA STICS crop growth model (Beaudoin et al., 2009), which includes the calculations of root front growth and root length growth. The root front growth is a function of temperature, with the depth of the root front beginning at the sowing depth for sown crops and at an initial value of transplanted crops or perennial crops (Beaudoin et al., 2009). The root length growth is calculated in each soil layer, considering the net assimilation rate and the allocation fraction of net assimilation to root, which is in turn a function of leaf area index (LAI) and root zone water content (Krinner et al. 2005). The root length density profile is then used to calculate the root resistance to water flow radially across the roots, soil hydraulic resistance, and plant axial resistance to flow from the soil to the leaves (see Appendix A.4).

2.4 STEMMUS-SCOPE v1.0.0 Coupling

The coupling starts with an initial soil moisture (*SM*) profile simulated by STEMMUS, which enables the calculation of the water stress factor as a reduction factor of the maximum carboxylation rate (V_{cmax}), SCOPE v1.73 is then used to calculate net photosynthesis (A_n) or gross primary productivity (*GPP*), soil respiration (*Rs*), energy fluxes (*Rn*, *LE*, *H* and *G*), transpiration (*T*) and *SIF*, which is passed to STEMMUS as the root water uptake (RWU). Then, the gross primary production (*GPP*) can be calculated based on A_n. Surface soil moisture is also used in calculating soil surface resistance and then calculating soil evaporation (*E*). Furthermore, SCOPE can calculate soil surface temperature (T_{s0}) based on energy balance, which was subsequently used as the top boundary condition of STEMMUS, and leaf water potential (*LWP*), which is a parameter to reflect plant water status, can be calculated through iteration. Based on RWU, STEMMUS calculates the soil moisture in each layer at the end of the time step, and the new soil moisture profile will be the soil moisture at the beginning of next time step, which is repeated as such till the end of simulation period. The time-step of STEMMUS-SCOPE is flexible and the time step used in this study was half hour. Figure 1 shows the coupling scheme of STEMMUS and SCOPE, and Table B.1 shows all the parameter values used in this study.

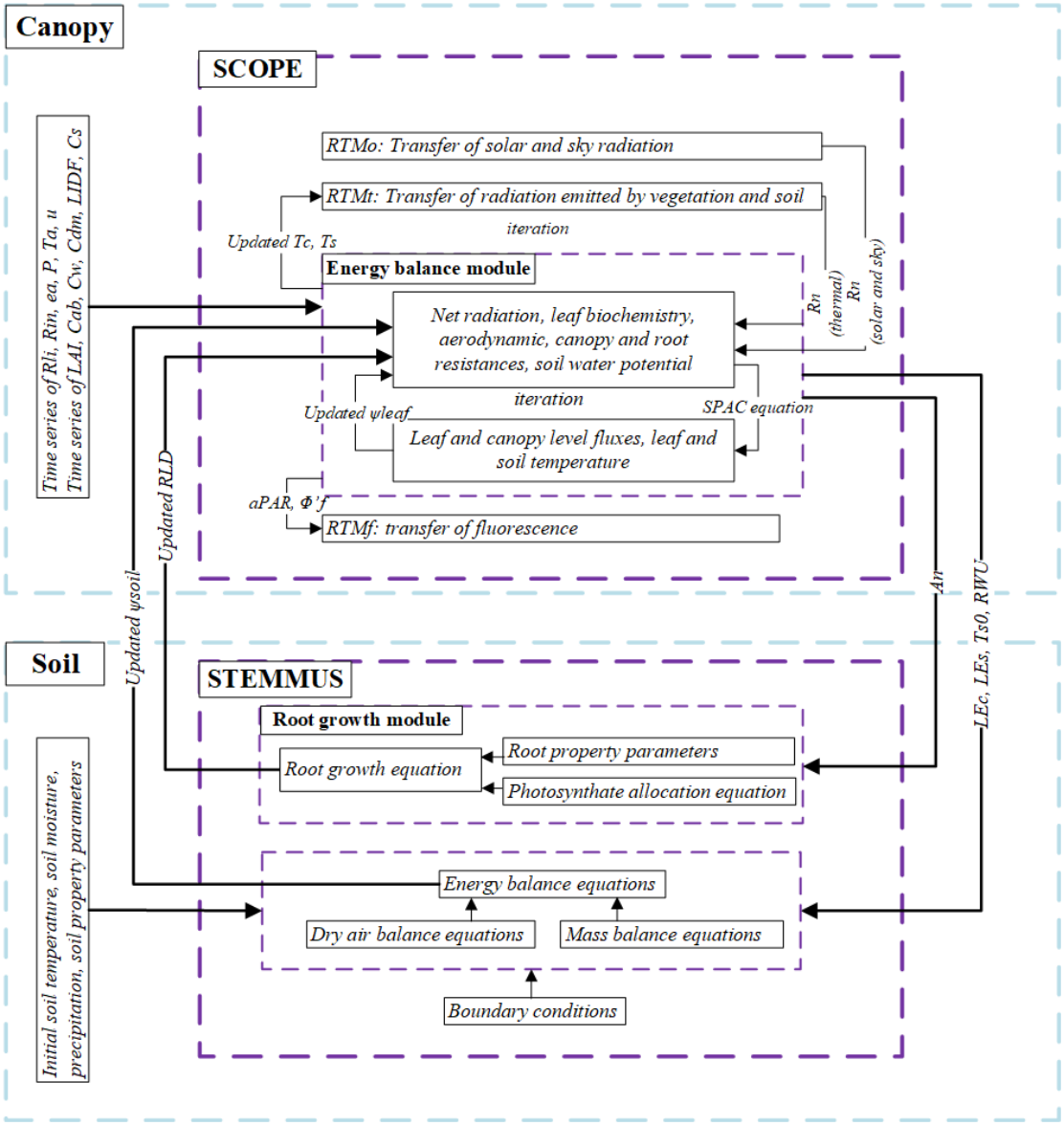

Figure 1. The coupling scheme of STEMMUS-SCOPE. The explanations of the symbols were the same as in Table B.1.

2.5. Evapotranspiration partitioning

Most studies in partitioning evapotranspiration (*ET*) use sap flow and micro lysimeter data from in-situ measurements. In this study, we used a simple and practical method to separate evaporation (*E*) and transpiration (*T*) proposed by Zhou et al. (2016). Although the behaviour of plant stomata is influenced by environmental factors, the potential water use efficiency ($uWUE_p$, g C $hPa^{0.5}$/kg H_2O) at stomatal scale in the ecosystem with a homogeneous underlying surface is assumed to be nearly constant, and variations of actual *uWUE* (g C $hPa^{0.5}$/kg H_2O) can be attributed to the soil evaporation (Zhou et al., 2016). Thus, the method can be used to estimate *T* and E with the quantities of *ET*, *uWUE* and $uWUE_p$. Another assumption of this method is that the ecosystem *T* equal to *ET* at some growth stages, so $uWUE_p$ can be estimated using the upper bound of the ratio of $GPP\sqrt{VPD}$ to *ET* (here VPD refers to vapor pressure deficit) (Zhou et al., 2014; Zhou et al., 2016).

Zhou et al. (2016) used the 95th quantile regression between $GPP\sqrt{VPD}$ and *ET* to estimate $uWUE_p$, and showed that the 95th quantile regression for $uWUE_p$ at flux tower sites was consistent with the *uWUE* derived at the leaf scale for different ecosystems. In addition, the variability of seasonal and interannual $uWUE_p$ was relatively small for a homogeneous canopy. Therefore, the calculations of $uWUE_p$, *uWUE*, and *T* at the ecosystem scale were as follows:

$$uWUE_p = \frac{GPP\sqrt{VPD}}{T} \quad (1)$$

$$uWUE = \frac{GPP\sqrt{VPD}}{ET} \quad (2)$$

$$\frac{T}{ET} = \frac{uWUE}{uWUE_p} \quad (3)$$

The calculation of *VPD* was based on air temperature and relative humidity data, and the method of gap-filling was the Marginal Distribution Sampling *(MDS)* method proposed by Reichstein et al. (2005). To calculate *GPP*, the complete series of net ecosystem exchange *(NEE)* was partitioned into gross primary production *(GPP)* and respiration *(Re)* using the method proposed by Reichstein et al. (2005). Finally, *ET* was calculated using the latent heat flux and air temperature. Based on *GPP*, *ET* and *VPD* data, *T* can be calculated using the method proposed by Zhou et al. (2016).

2.6. Study site and data description

To evaluate the performance of STEMMUS-SCOPE in modelling ecohydrological processes, simulation was conducted to compare STEMMUS-SCOPE with SCOPE, SCOPE_SM, and STEMMUS using observations over a C4 cropland (Summer-maize: from 11 June to 10 October 2017) at the Yangling station (34°17′ N, 108°04′ E, 521 m a.s.l.) and a C3 grassland at the Vaira Ranch (US-Var) Fluxnet site (38°25′ N, 120°57′ W, 129 m a.s.l.) (Annual grasses: from 1 June to 8 August 2004). The seasonal variation of precipitation, irrigation, and *SM* for these two sites were presented in Figure 2. And the ~~main~~ differences of soil surface resistance, water stress factor (*WSF*), *ET*, photosynthesis, soil surface temperature (T_s0), root water uptake

(RWU) and leaf water potential (*LWP*) between these four models were presented in Table 2. In this study, the LAI data of Vaira Ranch (US-Var) Fluxnet site was from MODIS 8-daily LAI product instead of the field measured LAI used by Bayat et al. (2019). For the soil water content used by SCOPE_SM, the averaged root zone soil moisture was used for Yangling station and the soil moisture at 10 cm depth was used for Vaira Ranch site. More detailed descriptions of these sites and data can refer to Wang et al. (2019; 2020a) and Bayat et al. (2018; 2019).

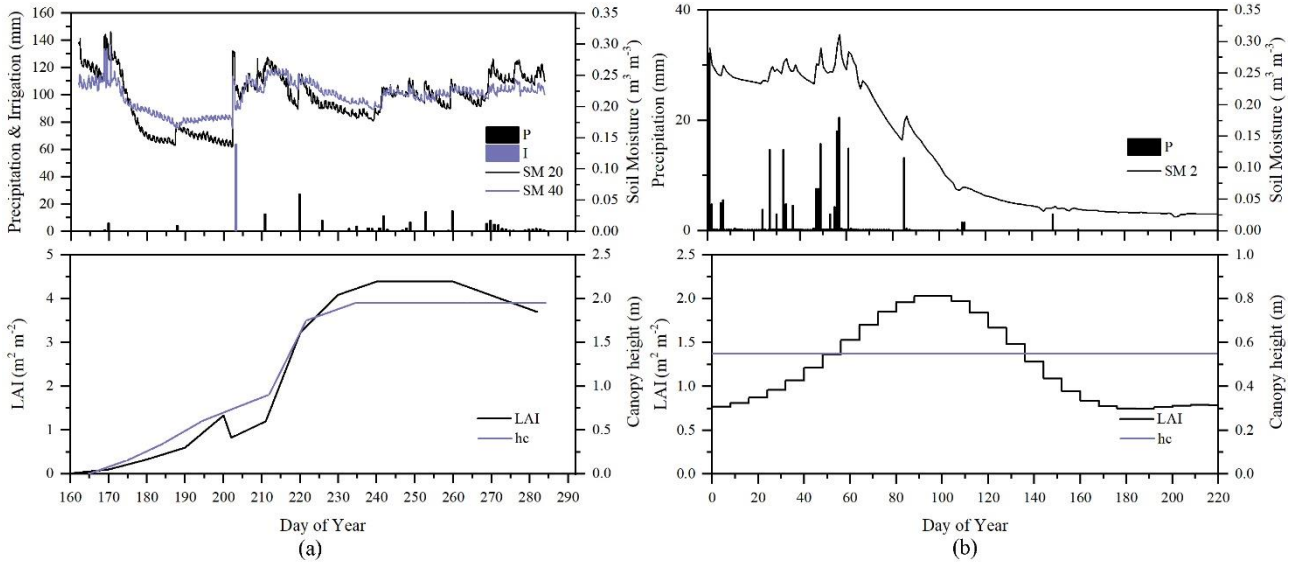

Figure 2 Seasonal variation of precipitation (P), irrigation (I), soil moisture at 2cm (SM 2), 20 cm (SM 20), 40 cm depth (SM 40), Leaf area index (LAI), and canopy height (h_c): (a) Maize cropland at Yangling station; (b) Grassland at Vaira Ranch (US-Var) Fluxnet site.

Table 2. Main differences among SCOPE, SCOPE_SM, STEMMUS, and STEMMUS-SCOPE.

	SCOPE	SCOPE_SM	STEMMUS	STEMMUS-SCOPE
Source	Van der Tol et al. (2009)	Bayat et al. (2019)	Zeng et al. (2013)	This study
*S*oil surface resistance calculation	Set *SM* as constant or field measured surface *SM*	Field measured surface *SM*	Simulated surface *SM* by itself	Simulated surface *SM* by itself
WSF calculation	Set *SM* as constant	Field measured *SM*	Simulated *SM* by itself	Simulated *SM* by itself
ET calculation	Process based (Analogy with Ohm's law)	Process based (Analogy with Ohm's law)	Penman–Monteith model or FAO dual crop coefficient method	Process based (Analogy with Ohm's law)
Photosynthesis	Farquhar and Collatz model	Farquhar and Collatz model	Absent	Farquhar and Collatz model
Radiation transfer	SAIL4 model	SAIL4 model	Based on Beer's law	SAIL4 model
T_s0	Simulated by itself	Simulated by itself	Field measured	Simulated by itself
RWU calculation	Absent	Absent	Based on potential *T*, root fraction, and soil moisture profile	Based on leaf and soil water potential
LWP calculation	Absent	Calculated by iteration	Absent	Calculated by iteration
Root growth	Absent	Absent	Empirical model	Process-based model

2.7. Performance Metrics

The metrics used to evaluate the performance of coupled STEMMUS-SCOPE model include: (1) Root Mean Squared Error (*RMSE*); (2) coefficient of determination (R^2); and (3) the index of agreement (*d*). They are calculated as:

$$RMSE = \sqrt{\frac{1}{n}\sum_{i=1}^{n}(P_i - O_i)^2} \quad (4)$$

$$R^2 = \frac{\left[\sum_{i=1}^{n}(P_i-\bar{P})(O_i-\bar{O})\right]^2}{\sum_{i=1}^{n}(P_i-\bar{P})^2\sum_{i=1}^{n}(O_i-\bar{O})^2} \quad (5)$$

$$d = 1 - \frac{\sum_{i=1}^{n}(P_i-O_i)^2}{\sum_{i=1}^{n}(|P_i-\bar{O}|+|O_i-\bar{O}|)^2} \quad (6)$$

where P_i is the *i*th predicted value, O_i is the *i*th observed value, $\bar{O}$ is the average of observed values, and *n* is the number of samples.

3. Results and discussion

3.1. Soil moisture modelling

As the soil moisture profile was not available in US-Var site, the comparisons of simulated soil moisture (*SM*) at Yangling station using STEMMUS and STEMMUS-SCOPE and observed ones are presented in Figure 3. For the simulation of soil moisture at 20 cm, the RMSE value was 0.023 and 0.021, and d value was 0.90 and 0.91, for STEMMUS and STEMMUS-SCOPE respectively. For the simulation of soil moisture at 40cm, the RMSE value was 0.017 and 0.021 and d value was 0.83

and 0.74, respectively. The simulated soil moisture at 20 cm depth agreed with the observed values in terms of seasonal pattern. Although slight overestimation occurred at initial and late stages, the dynamics in soil moisture resulted from precipitation or irrigation were well captured. Per the nature of the two models, the coupling of SCOPE with STEMMUS is not expected to improve the simulation of soil moisture. However, compared to SCOPE_SM, which used soil moisture measurements as inputs, the coupled STEMMUS-SCOPE improves the simulation of soil moisture dynamics as measured. The deviation between the model simulations and the measurements can be attributed to the following two potential reasons. First, the field observation has errors to a certain extent and the soil moisture sensors may be not well calibrated. Second, in this simulation, we assumed that the soil texture was homogeneous in the vertical profile, whereas the soil properties (e.g. soil bulk density and saturated hydraulic conductivity) may vary with depth in reality, and at different growth stages due to field management practices. For example, the soil bulk density at 40 cm was much higher than that at 20 cm due to the mechanical tillage, especially in the early stage.

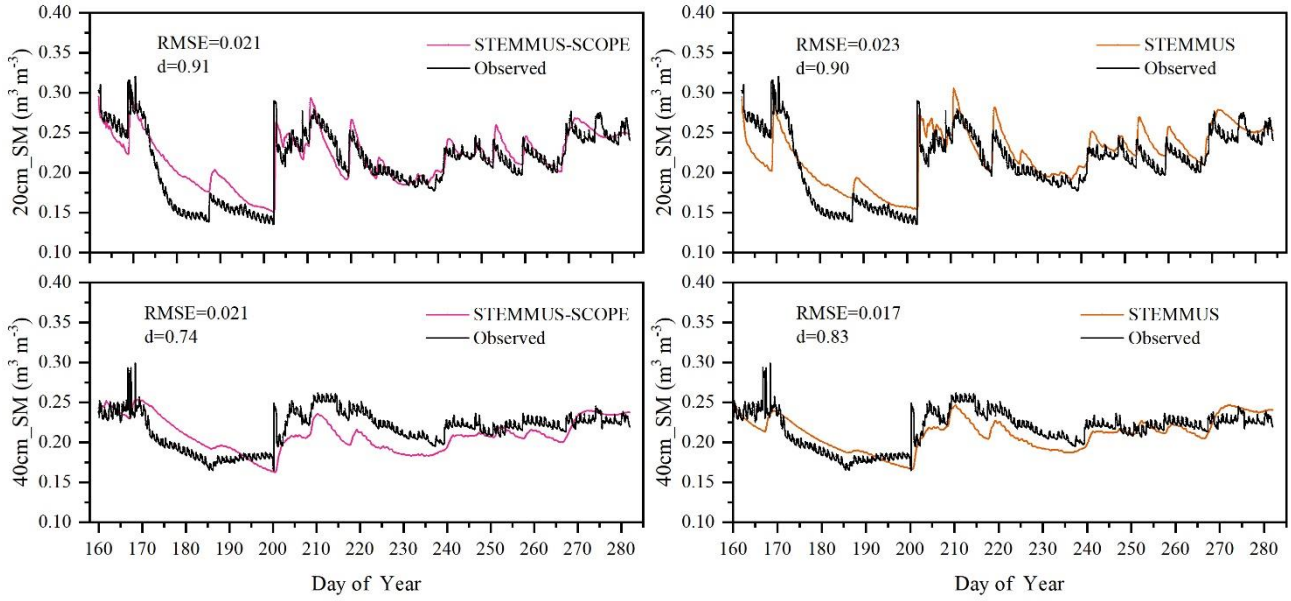

Figure 3 Comparison of modeled and observed soil moisture at 20 cm (20 cm_SM) and 40 cm depth (40 cm_SM) for the maize cropland at Yangling station.

3.2. Soil temperature modelling

Similar to soil moisture, only simulated soil temperatures (*Ts*) at Yangling site by STEMMUS and STEMMUS- SCOPE at 20 cm and 40 cm depth are shown in Figure 4. In general, both two models can capture the dynamics of soil temperature well. For the simulation of temperature at 20 cm, the RMSE value was 2.56 ºC and 2.58 ºC, and d value was 0.92 and 0.92, for STEMMUS and STEMMUS-SCOPE respectively. For the simulation of temperature at 40cm, the RMSE value was 2.06 ºC

and 2.07 ºC, and d value was 0.93 and 0.93, respectively. These results indicate that both models can simulate well soil temperature. However, there also exist some differences between simulation and observation. The largest difference occurred in DOY 202, when the field was irrigated with the flooding irrigation method. This irrigation activity may lead to the boundary condition errors (i.e., for soil surface temperature), which cannot be estimated well enough (e.g., there is no monitoring of water temperature from the irrigation). Meanwhile, the measurement may also have some errors in this period. The fact for the observed soil temperature at 20 cm and 40 cm decreasing to almost the same level at the same time indicates a potential pathway for preferential flow in the field (see precipitation/irrigation at DOY 202 in Figure 2), and the sensors captured this phenomenon. Nevertheless, the model captures the soil temperature dynamics.

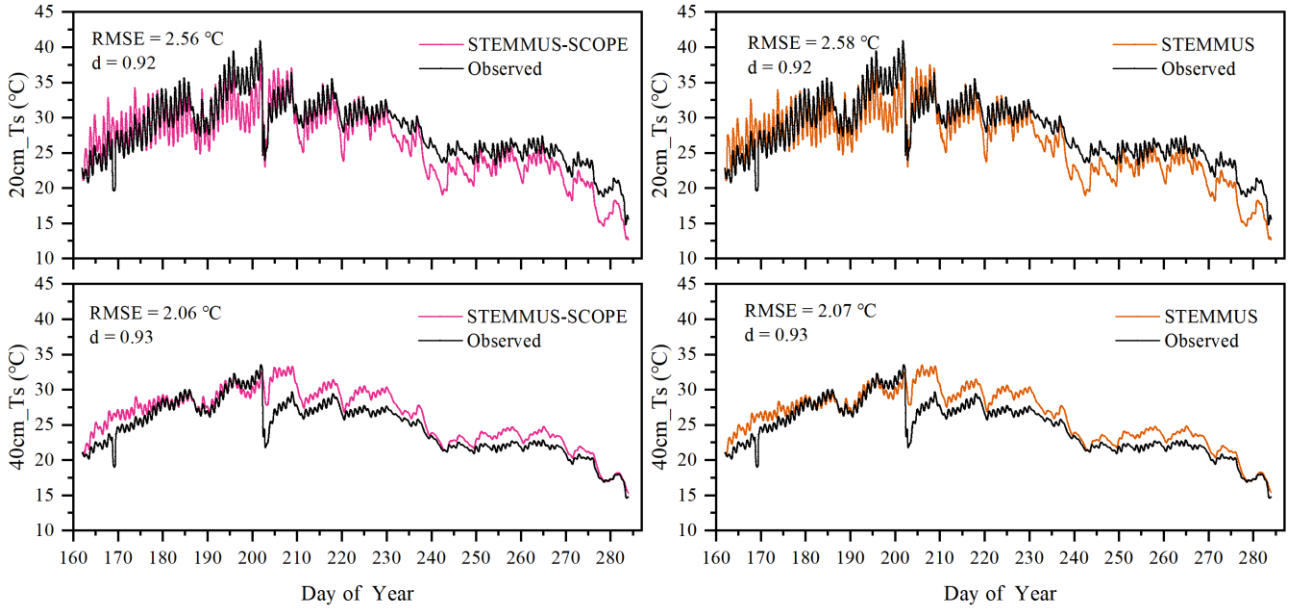

Figure 4 Comparison of observed and modeled soil temperature at 20 cm (20 cm_Ts) and 40 cm depth (40 cm_Ts) for the maize cropland at Yangling station.

3.3. Energy balance modelling

A comparison of the modeled and observed half-hourly net radiation (*Rn*), sensible heat flux (*H*), latent heat flux (*LE*), and soil heat flux (*G*) using SCOPE, SCOPE_SM, and STEMMUS-SCOPE are presented in Figure 5 (STEMMUS uses *Rn* as driving data and therefore is not included in the comparison). For net radiation and soil heat flux, the simulations of all three models show good agreements with observations, and the coefficient of determination (R^2) for SCOPE, SCOPE_SM and STEMMUS-SCOPE was 0.99, 1.00, and 0.99, respectively. For soil heat flux, the R^2 for SCOPE, SCOPE_SM and STEMMUS-SCOPE was 0.81, 0.79, and 0.80, respectively. For latent heat flux, STEMMUS-SCOPE has a better performance than SCOPE and SCOPE_SM, and the R^2 for SCOPE, SCOPE_SM and STEMMUS-SCOPE was 0.82, 0.84, and 0.85,

respectively. Furthermore, STEMMUS-SCOPE and SCOPE_SM have a similar performance in the simulation of sensible heat flux, which were better than the performance of SCOPE, and the R^2 for SCOPE, SCOPE_SM and STEMMUS-SCOPE was 0.70, 0.75, and 0.74, respectively.

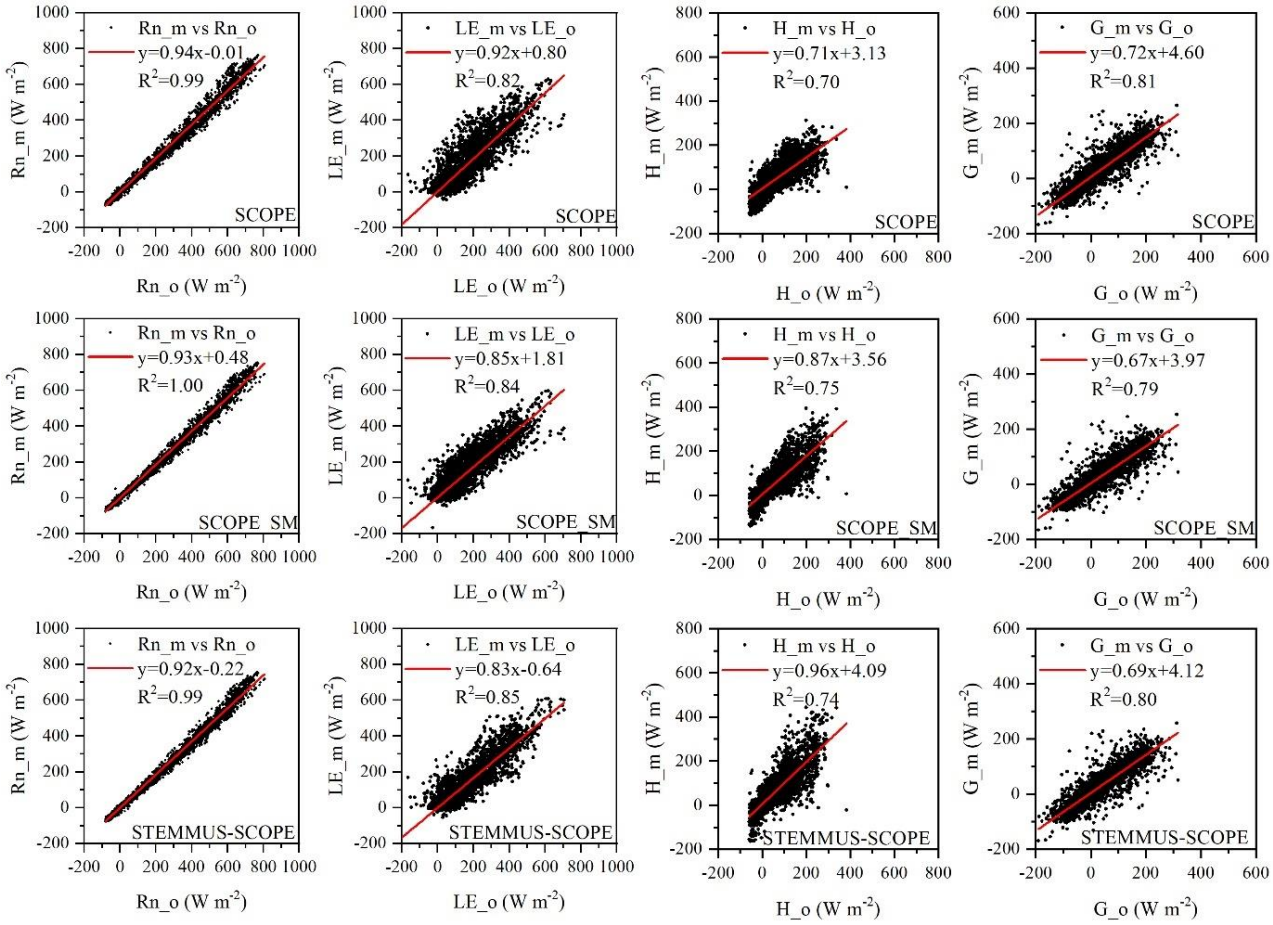

Figure 5 Comparison of modelled and observed half-hourly net radiation (Rn), latent heat (LE), sensible heat (H) and soil heat flux (G) by SCOPE, SCOPE_SM and STEMMUS-SCOPE at Yangling station. Subscripts '_m' and '_o' in each plot indicates modeled and observed quantities, respectively. The regression line is indicated in red color with the corresponding regression equation and the R^2.

3.4. Daily ET, T and E modelling

Simulated daily evapotranspiration (ET) results by SCOPE, SCOPE_SM, STEMMUS and STEMMUS-SCOPE are presented in Figure 6. For the Yangling station, the R^2 by SCOPE, SCOPE_SM, STEMMUS and STEMMUS-SCOPE was 0.76, 0.82, 0.80 and 0.81, and the *RMSE* was 0.84, 0.69, 0.76, and 0.74 mm day^{-1}, respectively. For the US-Var station, the R^2 by SCOPE, SCOPE_SM, STEMMUS and STEMMUS-SCOPE was 0.10, 0.66, 0.84 and 0.89 and the *RMSE* was 1.83, 0.63, 0.40, and 0.34 mm day^{-1}, respectively. For the ET simulation by SCOPE, there were large differences between simulations and observations

when the vegetation suffered water stress. For SCOPE_SM, STEMMUS and STEMMUS-SCOPE, because of including the dynamics of soil moisture, the simulated ET were closer to observations when the vegetation experienced water stress. It indicates that STEMMUS-SCOPE, STEMMUS and SCOPE_SM can predict ET with a relatively higher accuracy, especially when the maize was under water stress (DOY ~~193~~ 183 to 202 at Yangling station and DOY 90 to 220 at US-Var site), and STEMMUS-SCOPE and SCOPE_SM performed similarly well. It is noteworthy that although STEMMUS has considered the effect of soil moisture on ET, the accuracy of STEMMUS was lower than the coupled model (see Figure 6). The possible reason is the better representation of transpiration in SCOPE model (see Figure 7), which separates the canopy into 60 layers, while STEMMUS only treats the canopy as one layer. Besides, the coupled model performed better at grassland than at maize cropland. The reason is that the grassland simulation used the dynamic V_{cmax} data while the maize simulation used a constant V_{cmax} data.

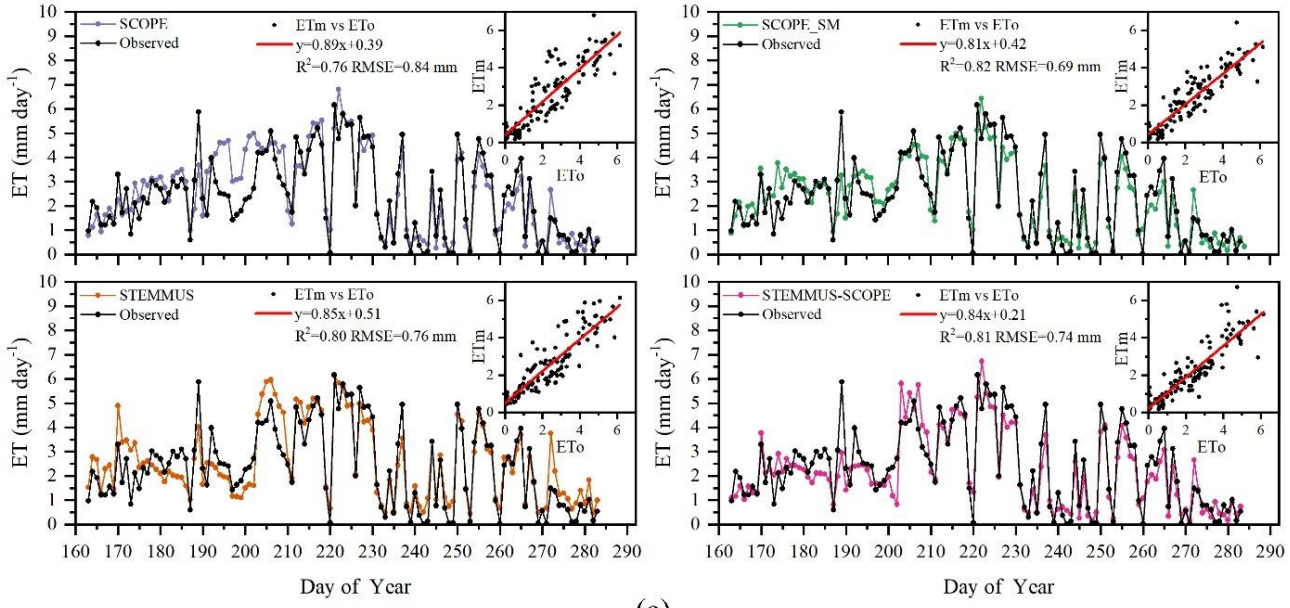

(a)

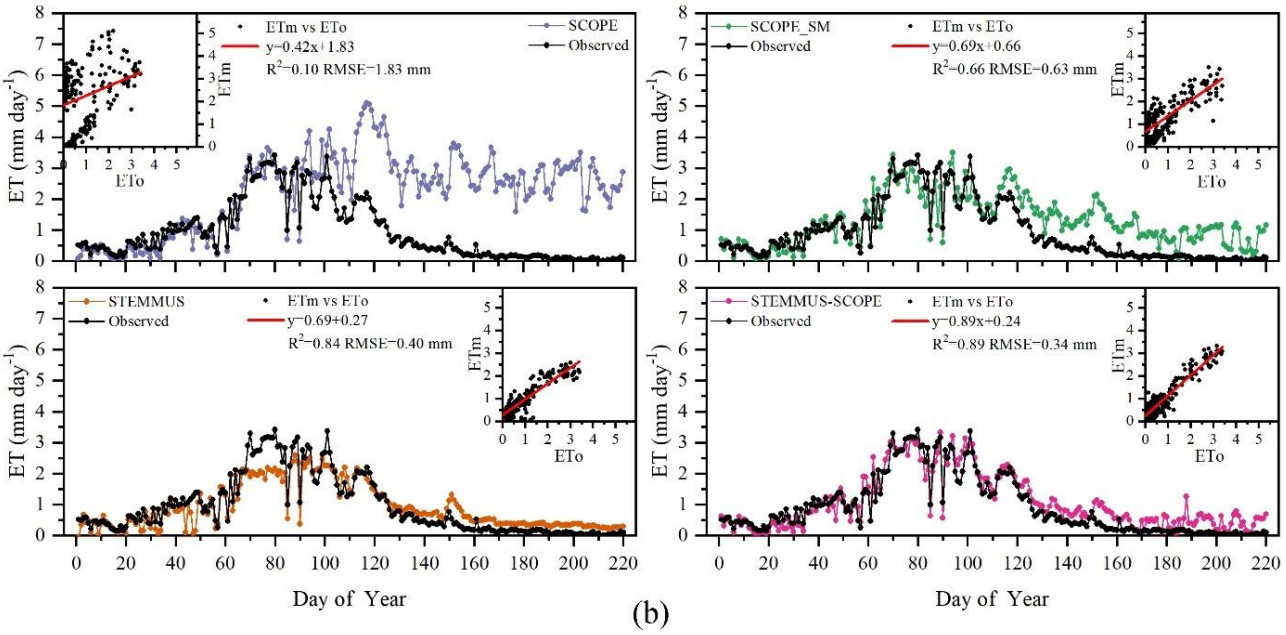

Figure 6 Comparison of modeled and observed daily evapotranspiration (ET): (a) Maize cropland at Yangling station; (b) Grassland at Vaira Ranch (US-Var) Fluxnet site. (ETm: modeled ET; ETo: observed ET).

The modeled and observed daily transpiration at maize cropland are presented in Figure 7 and the modeled transpiration at grassland is presented in Figure 8. For Yangling station, the R^2 value between simulated and observed transpiration was 0.82, 0.86, 0.79, and 0.86, and the *RMSE* was 0.60, 0.50, 0.67, and 0.50 mm day^{-1}, for SCOPE, SCOPE_SM, STEMMUS and STEMMUS-SCOPE, respectively. Because of ignoring the effect of water stress on transpiration, SCOPE failed to simulate transpiration accurately when the vegetation experienced water stress. As shown in the Figure 6(a), SCOPE overestimated transpiration for the maize cropland at Yangling station from DOY 183 to DOY 202 during the water stress period. Compared with SCOPE, SCOPE_SM, STEMMUS and STEMMUS-SCOPE can capture the reduction of transpiration during the dry period. The performances of STEMMUS-SCOPE and SCOPE_SM were also better than that of STEMMUS. The possible reason is the ~~better simulation~~more processed-based consideration of the radiative transfer and energy balance at leaf level in the coupled STEMMUS-SCOPE model (as also in SCOPE_SM) and the more accurate root water uptake (compared to that in SCOPE_SM). Nevertheless, STEMMUS-SCOPE slightly underestimated transpiration when the plant was undergoing severe water stress and slightly overestimated it after the field was irrigated. This is mainly because the actual V_{cmax} was not only influenced by drought but also related to leaf nitrogen content (Xu and Baldocchi, 2003), which was not considered in the maize cropland simulation. Although the measured T at the grassland was not available, we compared modeled T by the four models (Figure 7). During the wet season (before DOY 85), the modeled T by SCOPE, SCOPE_SM, and STEMMUS-SCOPE were similar and were higher than that by STEMMUS from DOY 64 to 82. During the dry season (after DOY 85), due to the simplified consideration of soil processes, the modeled T by SCOPE and SCOPE_SM were both much higher than that by

STEMMUS and STEMMUS-SCOPE. The reason for the better performance by the coupled model for the grassland (Figure 6(b)) is that it considers also the effect of leaf chlorophyll content (C_{ab}) on V_{cmax}, in addition to more detailed consideration of water stress as discussed above for the maize cropland.

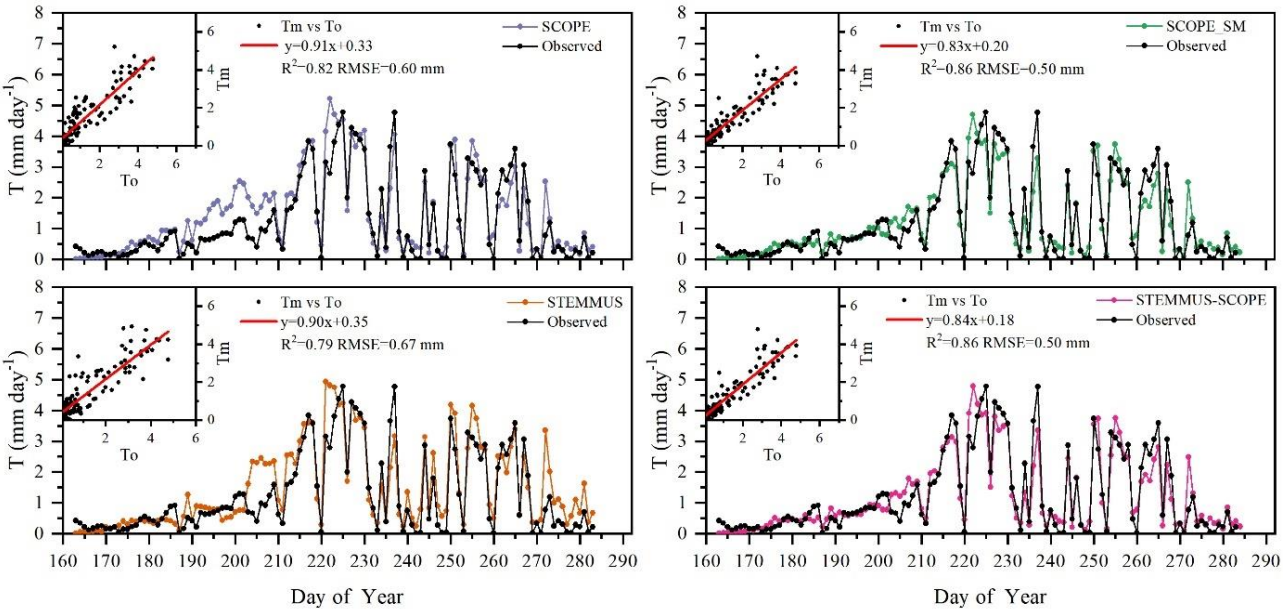

290

Figure 7 Comparison of modeled and observed daily plant transpiration (T) for the maize cropland at Yangling station (Tm: modeled T; To: observed T).

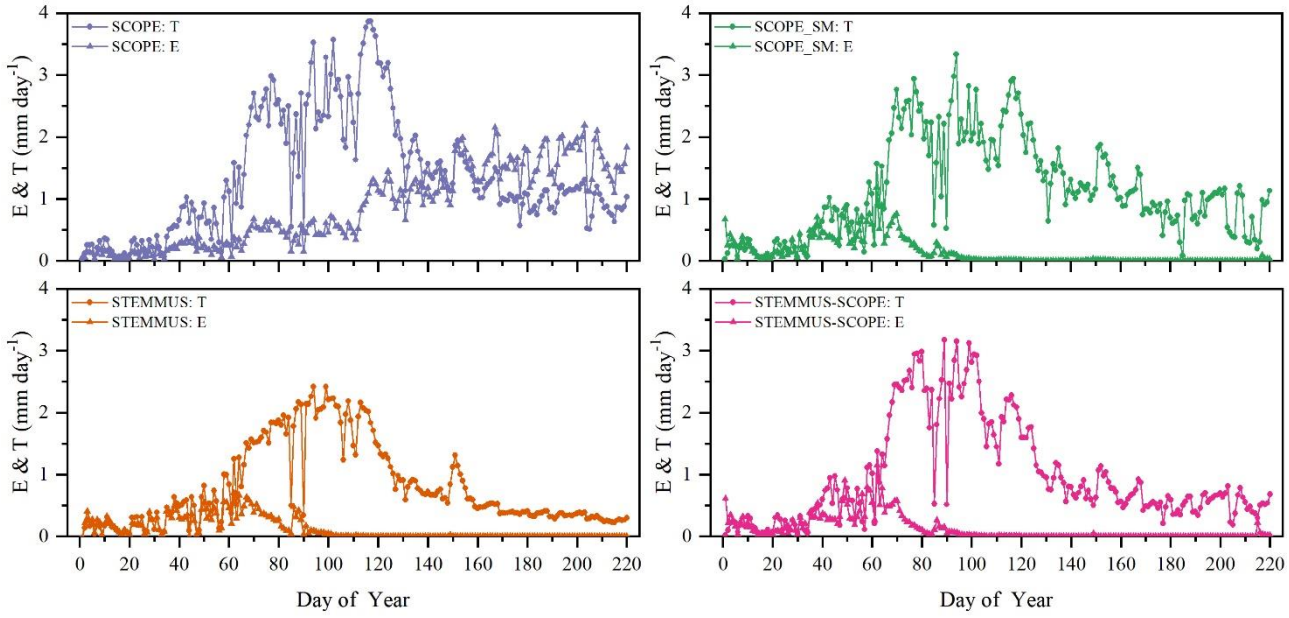

Figure 8 Comparison of modeled daily transpiration (T) and soil evaporation (E) for grassland at Vaira Ranch (US-Var) Fluxnet site (T: transpiration; E: soil evaporation).

As shown in Figure 9 for soil evaporation at Yangling station, the simulation by STEMMUS-SCOPE is closer to observation than those by other models. When using SCOPE to simulate soil evaporation, the soil moisture is set as constant (i.e., 0.25 m^3 m^{-3}). Therefore, SCOPE generally underestimates soil evaporation when soil moisture is higher than 0.25 and overestimates it when it is lower than 0.25. Here we use the average soil moisture at root zone simulated by STEMMUS-SCOPE as the input data for SCOPE and SCOPE_SM to calculate soil surface resistance and soil evaporation. Although STEMMUS can capture variation of soil evaporation reasonably well, it has higher *RMSE* value than STEMMUS-SCOPE. This is probably attributed to the comprehensive consideration of radiation transfer in SCOPE, which is lacking in STEMMUS. Consequently, the simulation of soil net radiation by the coupled model was more accurate than that by STEMMUS alone. The *RMSE* value by STEMMUS-SCOPE was 0.60 mm day^{-1}, which was lower than those by other three models (i.e. 0.67, 0.65, and 0.64 mm day^{-1} respectively). For STEMMUS-SCOPE, the major differences between simulations and observations occurred in rainy or irrigation days (cf. Figure 2(a)), which may be caused by errors of the estimated soil surface resistance during these periods or the uncertainty of ET partitioning method. The uncertainty of ET partitioning method (Zhou et al., 2016) was mainly caused by: (1) the uncertainty in the partitioning of *GPP* (less than 10%) and *Re* based on *NEE*, which would result in some uncertainty in *uWUE*; (2) due to the seasonal variation of atmosphere CO_2 concentration, the assumption of $uWUE_p$ being constant would cause some uncertainty (less than 3%); (3) the assumption of *T* being equal to *ET* sometimes during the growing season would cause some uncertainty when vegetation is sparse. Because the observed E at US-Var site was not available, a comparison of

only modeled E was shown in Figure 8, in which SCOPE modeled unrealistic E during the dry season, while the modeled E by SCOPE_SM, STEMMUS, and STEMMUS-SCOPE were consistent due to use the simulated surface *SM* as the input for soil evaporation calculation.

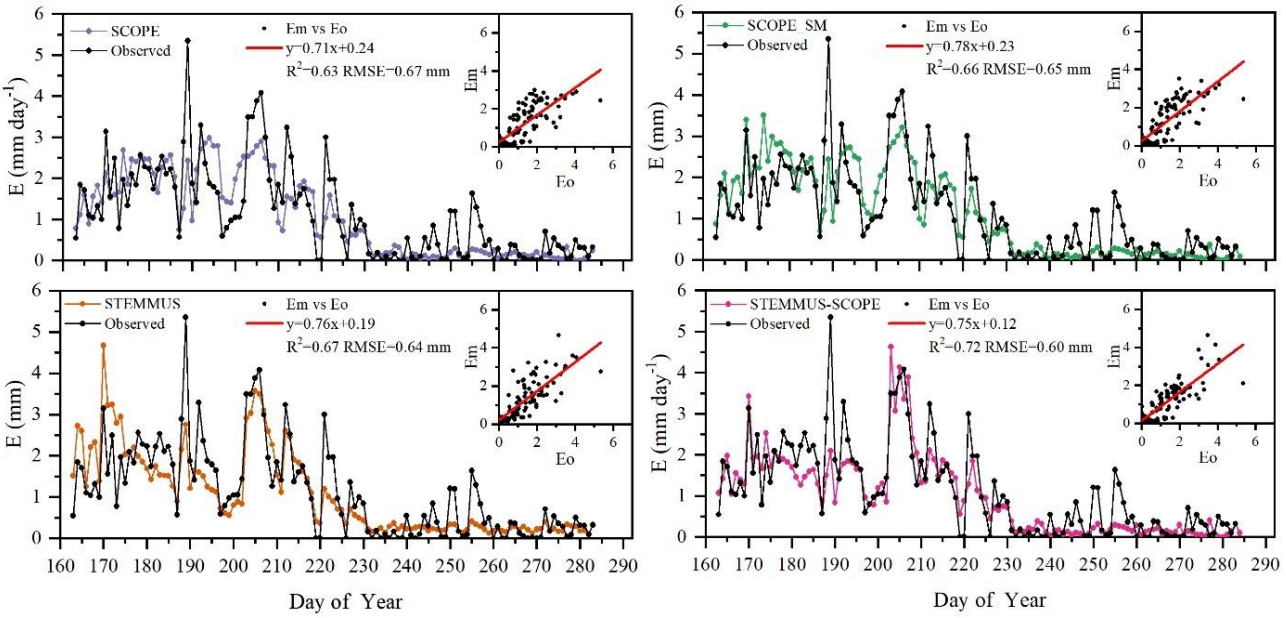

Figure 9 Comparison of modeled and observed daily soil evaporation (E) at Yangling station (Em: modeled E; Eo: observed E).

3.5. Daily GPP modelling

Simulated *GPP* by SCOPE, SCOPE_SM and STEMMUS-SCOPE and observed *GPP* are presented in Figure 10. As shown, similar to the simulation of transpiration, SCOPE cannot respond to water stress when simulating *GPP*. After introducing soil water stress factor in STEMMUS-SCOPE and SCOPE_SM, the simulations of *GPP* were improved in both models. For Yangling station, the consistency between simulated and observed *GPP* at mid and late stages were higher than those at early and rapidly growth stages. The difference usually occurred when soil moisture increased. For US-Var site, STEMMUS-SCOPE can simulate *GPP* well during the whole period, while SCOPE_SM slightly underestimated *GPP* around DOY 80 when this site transits from wet season to dry season. It indicates that only using the surface *SM* cannot reflect the actual root zone *SM* when the vegetation experiencing moderate water stress. Under such a condition, the hydraulic redistribution (HR) and compensatory root water uptake (CRWU) process enable the vegetation to utilize the water in deep soil layer. Only using the surface soil water content to calculate RWU in SCOPE_SM ignored the effect of HR and CRWU process, and the effect of water stress was overestimated. However, the surface soil moisture can reflect root zone soil moisture well when the vegetation was not under water stress or severe water stress. A similar underestimated of *GPP* was also found by Bayat et al. (2019).

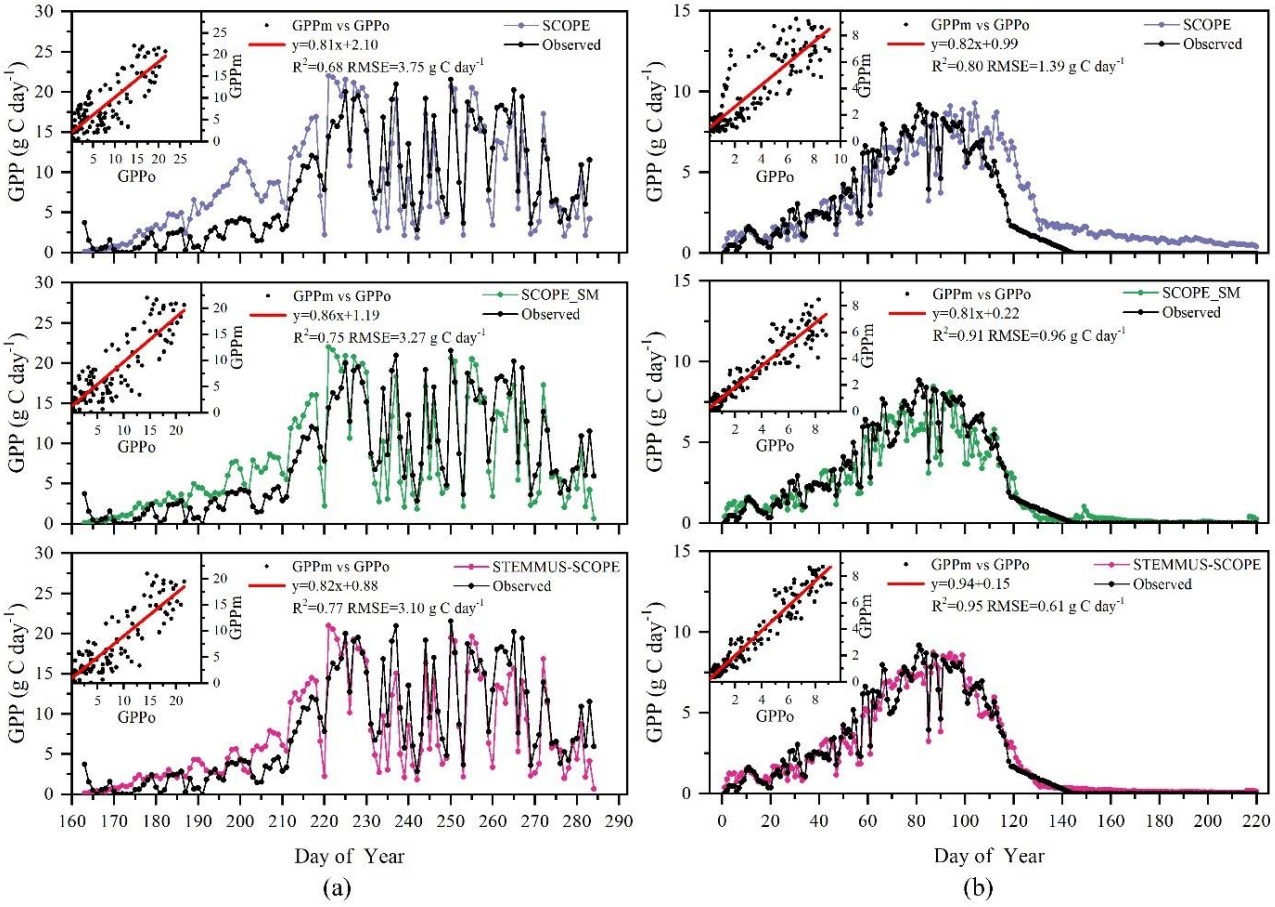

Figure 10 Comparison of modeled and observed daily gross primary production (GPP): (a) Maize cropland at Yangling station; (b) Grassland at Vaira Ranch (US-Var) Fluxnet site. (GPPm: modeled GPP; GPPo: observed GPP).

3.6. Simulation of leaf water potential (LWP), water stress factor (WSF), and root length density (RLD)

335 ~~Leaf water potential is a parameter to reflect plant water status.~~ The simulated half-hourly leaf water potential and water stress factor at Yangling station are presented in Figure 11. The leaf water potential was lower when vegetation suffering water stress compared to other periods. The reason is that soil water potential is low due to the low soil moisture and the plants need to maintain an even lower leaf water potential to suck water from the soil and transfer it to leaves. During mid and late stages, the leaf water potential was sensitive to transpiration demand due to the slowdown of root system growth. As the continuous 340 measurements of the leaf water potential is not available, we compared only the magnitude of simulated leaf water potential to measurements reported in literature.

Many studies have measured midday leaf water potential or dawn leaf water potential. Fan et al. (2015) reported that the leaf water potential of well-watered maize was maintained high between -73 to -88 m and leaf water potential would decrease

when soil water content was lower than 80% of field capacity. Martineau et al. (2017) reported the midday leaf water potential of well-watered maize was around -~~82~~ -0.82 MPa (about 84.8 m in water pressure head; note: 0.1MPa equal to 10.339 m water pressure head) and the midday leaf water potential decreased to -~~130~~ -1.3 MPa (about 134.4 m in water head) when the maize was suffering water stress. Moreover, O'Toole and Cruz (1980) studied the response of leaf water potential to water stress in rice and concluded that the leaf water potential of rice can be lower than -80 to -120 m when the vegetation was under water stress and the leaves started curling, which was similar to the simulated leaf water potential of maize in this study. Aston and Lawlor (1979) revealed the relationship between transpiration, root water uptake and leaf water potential of maize. These field studies found that leaf water potential was often very low and reached trough values at midday. Elfving (1972) developed a water flux model based on SPAC system, evaluated it for orange tree, and reported about -120 m for the trough value of leaf water potential under non-limiting environmental conditions, which was slightly lower than the simulation in this study.

In this study, the calculation of water stress factor considered the effect of soil moisture and root distribution. The severe water stress occurred from DOY ~~193~~ 183 to DOY 202, and the coupled model performed very well in this period. As the feedback, water stress can also influence root water uptake and root growth, and consequently influence soil moisture and root dynamics in next time step. It indicates that the water stress equation used in this study can characterize the reduction of V_{cmax} reasonably well.

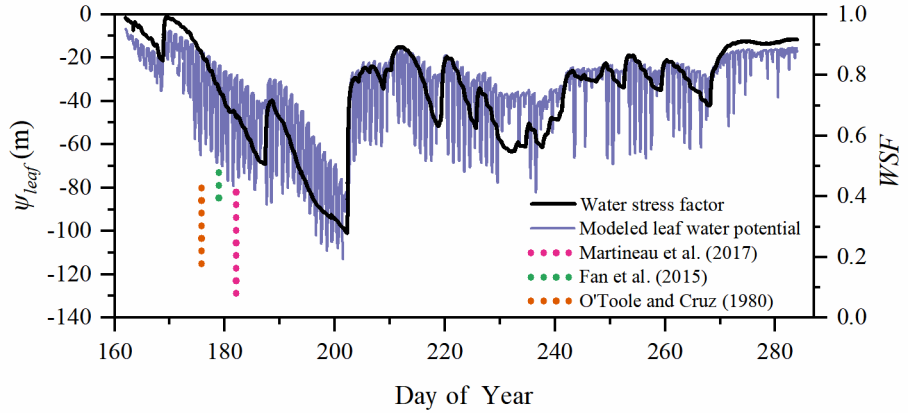

Figure 11 Simulation of ψ_{leaf} (leaf water potential, m) and *WSF* (water stress factor) at Yangling station. (The dashed lines represent the range of midday leaf water potential reported in other sites.)

Root length density is another vital parameter in calculating root water uptake. As shown in Table 3, the simulated peak root length density and maximum rooting depth of maize at Yangling station was ~~high in soil depth from 10 to 20 cm and gradually decreased from 20 cm to 121 cm~~ comparable to the measured values at other sites. Many previous studies revealed that root length density was influenced by soil moisture, bulk density, tillage, and soil mineral nitrogen (Amato and Ritchie, 2002; Chassot et al., 2001; Schroder et al., 1996). In this study, as we assumed the soil was homogenous, STEMMUS-SCOPE considered the effect of soil moisture but neglected the effect of bulk density and soil mineral nitrogen. Amato and Ritchie

(2002) also found a similar result as this study about the root length density in a maize field. Peng et al. (2012) studied temporal and spatial dynamics in root length density of field-grown maize and found that 80% root length density was distributed at 0-30 cm depth with peak values from 0.86 to 1.00 cm cm^{-3}. Ning et al. (2015) also reported a similar observation of root length density. Chassot et al. (2001) and Qin et al. (2006) reported that root length density can reach 1.59 cm cm^{-3} at Swiss midlands. In Stuttgart, Germany, Wiesler and Horst (1994) observed the root growth and nitrate utilization of maize under field condition. The observed root length density was 2.45-2.80 cm cm^{-3} at 0-30 cm depth which was much higher than in other studies, and decreased to 0.01 cm cm^{-3} at 120-150 cm depth, which was consistent with the observation of Oikeh et al. (1999) at Samaru, Nigeria. Zhuang et al. (2001b) proposed a scaling model to estimate the distribution of root length density of field grown maize. In their study, measured root length density in Tokyo, Japan decreased from 0.4-0.95 cm cm^{-3} at top soil layer to about 0.1 cm cm^{-3} at the bottom layer. Zhuang et al. (2001a) observed that the root length density of maize was mainly distributed at 0-60 cm depth and the maximum values were about 0.9 cm cm^{-3}. These studies indicated that the root length density values were quite variable when it was observed at different sites, nevertheless the simulated root length density in our study was in order of magnitude similar to the observations in previous studies (Table 3).

Table 3 Comparison of the peak root length density (RLD) (cm cm^{-3}) at Yangling station with that at other sites.

Location	Maximum rooting depth (cm)	Peak *RLD* (cm cm^{-3})	Soil type	Bulk density (g cm^{-3})	References
Potenza, Italy	100	0.84	Clay-loam	1.59-1.69	Amato and Ritchie (2002)
Beijing, China	60	0.78	Silty loam		Peng et al. (2012)
Alize, Stuttgart, Germany	150	2.45	Clay	1.5-1.7	Wiesler and Horst (1994)
Brummi, Stuttgart, Germany	150	2.80	Clay	1.5-1.7	Wiesler and Horst (1994)
Swiss midlands	100	1.59	Sandy silt	1.21-1.55	Qin et al. (2006)
Samaru, Nigeria	90	2.78	Loamy soil	1.39-1.67	Oikeh et al. (1999)
Tokyo, Japan	58	0.95	Sandy loam	0.61-0.80	Zhuang et al. (2001a, b)
Yangling, China	121	0.74	Sandy loam	1.41	This study

3.7. Diurnal variation of T, GPP, SIF, and LWP

Figure 12 shows the modeled and observed half-hourly canopy transpiration (*T*), gross primary production (*GPP*), solar-induced fluorescence (*SIF*) and leaf water potential (*LWP*) from DOY 183 to 202 at Yangling station. The simulations by STEMMUS-SCOPE and SCOPE_SM were consistent with observation while that by SCOPE was much higher than observation. The performances of STEMMUS-SCOPE and SCOPE_SM were consistent with that of SCOPE in the early morning and late afternoon, when the photosynthesis was mainly limited by incident radiation rather than by water stress, intercellular CO_2 concentration and V_{cmax}. In the midday, with increasing incident radiation, the photosynthesis was mainly limited by water stress and V_{cmax}, exactly when the simulations by STEMMUS-SCOPE and SCOPE_SM were much better

than that by SCOPE. The diurnal variation of observed and modeled *GPP* were similar to that of T. Due to lack of observed *SIF*, only the simulated *SIF* were presented. As the figure shown, the *SIF* simulated by STEMMUS- SCOPE and SCOPE_SM were reduced when the vegetation experiencing water stress, which indicated that both the simulated *SIF* of STEMMUS-SCOPE and SCOPE_SM can respond to water stress. However, the accuracy of the simulated *SIF* needs further validation with field observation.

Figure 13 shows the relationship among half-hourly *GPP*, *SIF*, and *LWP* on DOY 199 at Yangling station. There was a strong linear relationship between *SIF* and *GPP* when the maize was well-watered (Figure ~~14a~~13a). However, *SIF* kept increasing while *GPP* tended to saturate when the maize suffering water stress. This result is consistent with the previous study conducted for cotton and tobacco leaves (Van der Tol et al., 2014). Because SCOPE_SM used the averaged root zone *SM* and ignored vertical root and soil water distribution, it overestimated *GPP* and *SIF*. When the maize was experiencing drought, the *LWP* was maintained at a low level. With *GPP* and T increasing, the plant decreased *LWP* in order to extract enough water from the root zone. SPAC system enabled STEMMUS-SCOPE simulate half-hourly *LWP*~~-~~. To better detect the response of simulated *SIF* to simulated *LWP*, we choose a cloudless day (DOY 199) and a liner relationship between the simulated *SIF* and *LWP* was obtained (Figure ~~14b~~13b). Sun et al. (2016) reported that *SIF*-soil moisture-drought relationship depended on variations of both absorbed *PAR* and fluorescence yield in response to water stress, while the *LWP* can reflect both effect of absorbed *PAR* and soil moisture status. The strong correlation between *GPP*, *LWP* and *SIF* indicates a potential of using *SIF* as an effective signal for characterizing the response of photosynthesis to water stress. In the future, more studies should focus on the measurements of *SIF*, *GPP*, and *LWP* simultaneously for different vegetation types across different environmental conditions (radiation, soil moisture, and CO_2 concentration) to reveal how the water stress affects these relationships.

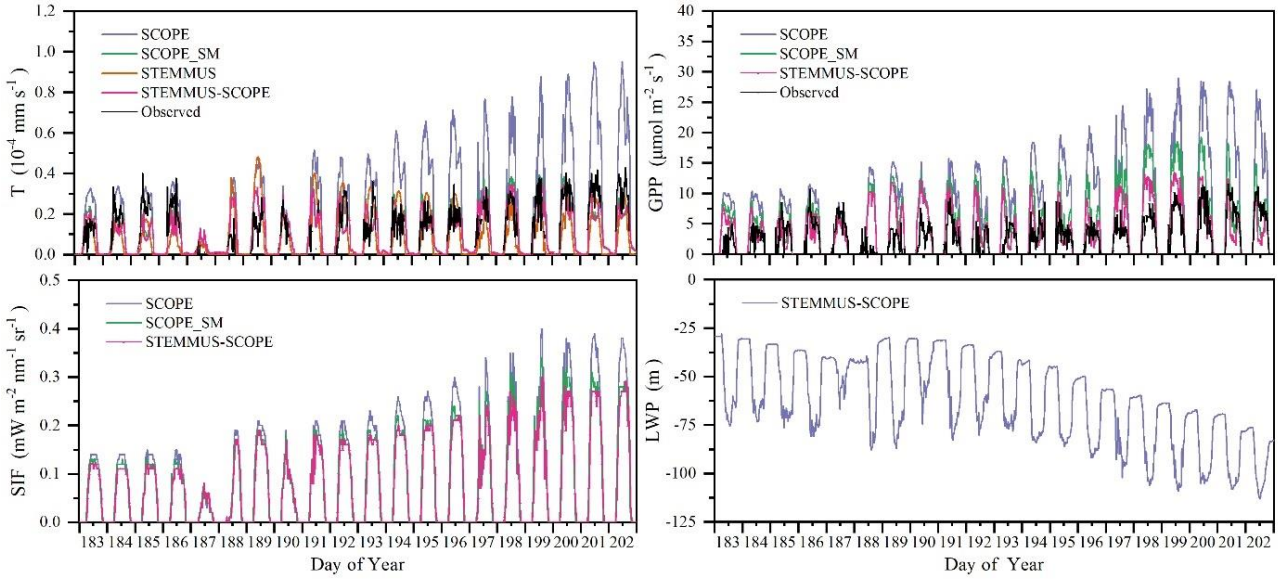

410 **Figure 12 Comparison of modeled and observed half-hourly transpiration (T), gross primary production (GPP), top of canopy solar-induced fluorescence (SIF) and leaf water potential (LWP) at Yangling station.**

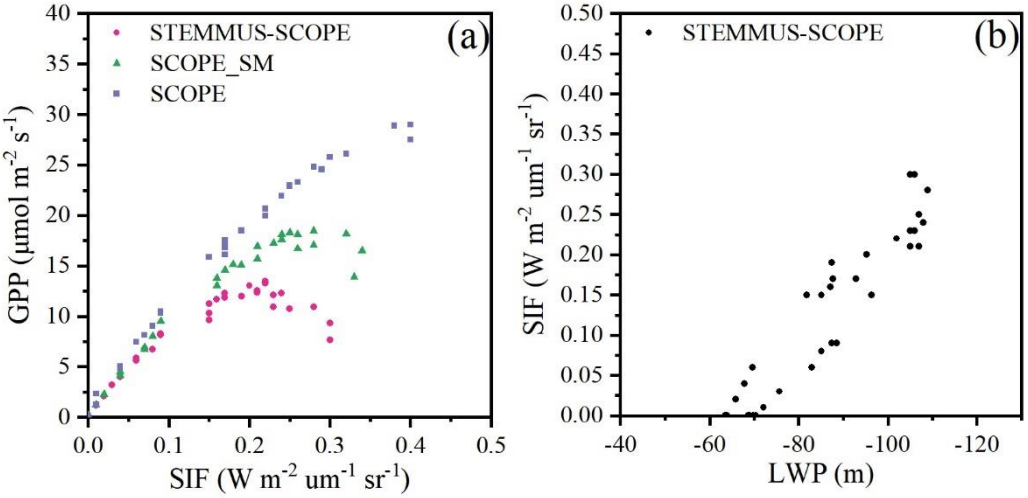

Figure 13 The relationship among gross primary production (GPP), top of canopy solar induced fluorescence (SIF), and leaf water potential (LWP) on DOY 199: (a) GPP vs SIF; (b) SIF vs LWP.

3.8. Limitations need to be overcame

The new coupled model notably improved simulations of carbon and water fluxes when vegetation suffering water stress. However, this study mainly aimed to improve the response of SCOPE to drought by introducing vertical soil water and root profile. Some critical processes were followed that existed in SCOPE_SM and STEMMUS. As with any model, some modules in STEMMUS-SCOPE, such as plant hydraulics and root growth, could be improved upon in future development.

First, to date many LSMs (e.g. CLM 5, Noah-MP, JULES, and CABLE) have incorporated state-of-the-art plant hydraulics model to replace the conventional empirical plant hydraulic model which was only based on the distribution of *SM* and fraction of roots (e.g. CLM 4.5 and CoLM) (De Kauwe et al., 2015). Although STEMMUS-SCOPE integrated a 1D root growth model and a relatively novel RWU model, its hydraulics model followed that in SCOPE_SM and ignored the most exciting recent advances in our understanding of plant hydraulics: hydraulic failure due to loss of hydraulic conductivity due to embolism and refilling for recovery from xylem embolism (McDowell et al., 2019). Because STEMMUS-SCOPE performed well in maize cropland and grassland, the influence of embolism and refilling on water transfer from the soil through vegetation to the atmosphere cannot be fully detected. The value of using plant water potential instead of soil water potential to constrain model predictions has been demonstrated in many case studies (De Kauwe et al., 2020; Niu et al., 2020; Medlyn et al., 2016; Xu et al., 2016; Williams et al., 1996). Niu et al. (2020) followed the plant hydraulic model developed by Xu et al. (2016) and represented plant stomatal water stress factor as a function of the plant water storage. CLM 5.0 also introduced a new formulation for *WSF*, which is based on leaf water potential (ψ_l) instead of soil water potential (ψ_s) (Kennedy et al., 2019). These new formulations based on plant water potential could have significant improvements for plant drought responses. Besides, STEMMUS-SCOPE presently does not account for plant water storage that may result in underestimating morning *LE* and overestimating afternoon *LE*. Some field observations showed that the plant did not immediately respond when soil moisture was enhanced (Mackay et al., 2019), but there are long lags, which was ignored in this study too, between soil water recovery from drought and plant responses to the recovery. The *WSF* in STEMMUS-SCOPE directly comes from soil moisture and cannot reflect true stomatal response when vegetation experiencing drought. For example, in early morning, the low stomatal aperture was induced by low *PAR* rather than by *SM*. Consequently, STEMMUS-SCOPE needs to introduce the advanced hydraulics when the model was tested in a wide range of ecosystems, particularly for vegetation exposed to frequent drought cycles or prolonged periods of severe drought events. It is important however to note that explicit representations of plant hydraulics require additional model parameters and increase parameterization burden. This is the most challenging limitation to STEMMUS-SCOPE for incorporating these hydraulics models and we have chosen a trade-off between mechanism and practicality.

Second, as mentioned above, STEMMUS-SCOPE adapted the macroscopic RWU model and a simplified 1D root growth model for saving computational costs, though it well predicted maximum root depth which is the most critical factor when calculating *WSF* and RWU. Such a simplification would likely ease the migration of our model into larger-scale models, such

as earth system models. However, STEMMUS-SCOPE oversimplified metabolic processes of the roots that include root exudates, root maintenance respiration, root growth respiration, and root turnover, which are also critical and have been incorporated in Noah-MP (Niu et al., 2020). This simplification could result in uncertainties in modelling the root growth and root water uptake. Meanwhile, there was no validation of seasonal vertical root length distribution based on in-situ observation, which need to be validated in the next step. Furthermore, the model presently does not account for the feedback between hydraulic controls over carbon allocation and the role of root growth on soil-plant hydraulics, which could also be considered in future model development.

4. Conclusions

A fundamental understanding of coupled energy, water and carbon flux is vital for obtaining the information of ecohydrological processes and functioning under climate change. The coupled model, STEMMUS-SCOPE, integrating radiative transfer, photochemistry, energy balance, root system dynamics, and soil moisture and soil temperature dynamics, has been proven to be a practical model to simulate detailed land surface processes such as evapotranspiration and *GPP*. In the coupled model, STEMMUS could provide root zone moisture profile to SCOPE, which was used to calculate water stress factor. On the other hand, SCOPE can provide net carbon assimilation and soil surface temperature to STEMMUS, which was used subsequently as the top boundary condition and as the input for root growth model. This study explores the role of dynamic root growth in affecting canopy photosynthesis activities, fluorescence emissions and evapotranspiration, which has not been reported before. The coupled model has been successfully applied in a maize field and a grassland, and can be used to describe ET partitioning, canopy photosynthesis, reflectance, and fluorescence emissions. The results show that via considering dynamic root growth and the associated root water uptake, the simulated *SIF* of the coupled STEMMUS-SCOPE model can ~~reflect and capture realistically the *SIF* variation during~~response to water stress~~ condition~~, while this is not the case for ~~SCOPE and~~ SCOPE_SM.

Through the inter-comparison of SCOPE, SCOPE_SM, STEMMUS, and STEMMUS-SCOPE, we concluded that the coupled STEMMUS-SCOPE can be used to investigate vegetation states under water stress conditions, and to simultaneously understand the dynamics of soil heat and mass transfer, as well as the root growth. By considering vertical distribution of soil moisture and root system, the simulation of water and carbon fluxes, especially when vegetation suffering moderate water stress, was significantly improved. However, there remain some needs for further studies to enhance the capacity of STEMMUS-SCOPE in understanding ecosystem functioning. Frist of all, the estimation of soil boundary condition especially during the irrigation period, which has significant influence on the simulation of soil temperature, needs further considerations. Second, the realism of the present model in modelling water-stressed *SIF* are subject to further studies. Nevertheless, STEMMUS-SCOPE may be used as an effective ~~observation operator~~forward simulator to simulate remote sensing signals and to assimilate remote sensing data such as solar-induced chlorophyll fluorescence, to improve the estimation of water and

carbon fluxes. STEMMUS-SCOPE could also be used to investigate regional or global land surface processes, especially in arid and semi-arid regions, due to its sensitivity to water stress conditions.

Code and data availability. The development and validation of STEMMUS-SCOPE in this paper were conducted in MATLAB R2016a. The exact version of the model used to produce the results used in this paper is archived on Zenodo (Wang et al., 2020). The original source of the SCOPE model and STEMMUS model was obtained from Van der Tol et al. (2009) and Zeng et al. (2011a, b), respectively. The tower-based eddy-covariance measurements used for model validation were obtained from the authors for the Yangling station, China (Wang et al., 2019), from the FLUXNET2015 Dataset and PLUMBER2 program for the Vaira Ranch (US-Var) Fluxnet site.

Author contributions. YW, YZ, HC and ZS designed the study, YW developed the code, conducted the analysis, and wrote the manuscript, YW and HC collected and shared their eddy-covariance measurements for the purpose of model validation. All authors discussed, commented and contributed to the revisions and final version of the manuscript.

Competing interests. The authors declare that they have no conflict of interest.

Acknowledgments. This work was supported by the National Natural Science Foundation of China (51879223 and 41971033), the National Key Research and Development Program of China (2016YFC0400201), the Fundamental Research Funds for the Central Universities, CHD (300102298307), and China Scholarship Council. Peiqi Yang was supported by the Netherlands Organization for Scientific Research, grant ALWGO.2017.018.

Appendix A

A.1. Photosynthesis and evapotranspiration under water stress in SCOPE

The C4 Photosynthesis is calculated in the SCOPE model as the minimum of three processes (Collatz et al., 1991; 1992); (1) carboxylation rate limited by Ribulose biphosphate-carboxylase-oxygenase activity (known as Rubisco (enzyme)-limited, V_c, described in Eq. (A1); (2) carboxylation rate limited by Ribulose 1–5 bisphosphate regeneration rate (known as RuBP (electron transport/light)-limited), V_e, described in Eq. (A2); (3) at low CO_2 concentrations, carboxylation rate limited by intercellular CO_2 partial pressure (p_i), V_s, described in Eq. (A3).

$$V_c = V_{cmax} * WSF \quad \text{(A1)}$$

$$V_e = \frac{J}{6}\frac{-b\pm\sqrt{b^2-4ac}}{2a} \quad \text{(A2)}$$

$$V_s = p_i(k_p - \frac{L}{p_i})/P \quad \text{(A3)}$$

$$A_n = min(V_c, V_e, V_s) \quad \text{(A4)}$$

The C3 Photosynthesis is calculated in the SCOPE model as the minimum of two processes (Farquhar et al., 1980); (1) carboxylation rate limited by Ribulose biphosphate-carboxylase-oxygenase activity (known as Rubisco (enzyme)-limited, V_c, described in Eq. (A5); (2) carboxylation rate limited by Ribulose 1–5 bisphosphate regeneration rate (known as RuBP (electron transport/light)-limited), V_e, described in Eq. (A6).

$$V_c = V_{cmax} * WSF * \frac{C_i-\Gamma^*}{C_i+K_c(1+\frac{O_i}{K_o})} \quad \text{(A5)}$$

$$V_e = \frac{J(C_i-\Gamma^*)}{4(C_i+2\Gamma^*)}\frac{-b\pm\sqrt{b^2-4ac}}{2a} \quad \text{(A6)}$$

$$A_n = min(V_c, V_e) \quad \text{(A7)}$$

$$C_i = C_a(1 - \frac{1}{mRH}) \quad \text{(A8)}$$

where V_{cmax} is the maximum carboxylation rate (μmol m^{-2} s^{-1}), p_i is the intercellular CO_2 partial pressure (Pa), k_p is a pseudo-first-order rate constant for PEP carboxylase with respect to C_i, P is the atmospheric pressure; A_n is the net photosynthesis (μmol m^{-2} s^{-1}); WSF is the total water stress factor, J is the electron transport rate (μmol m^{-2} s^{-1}), C_i is the intercellular CO_2 concentration (μmol m^{-3}) and C_a is CO_2 concentration in the boundary layer (μmol m^{-3}), m is Ball-Berry parameter and RH is relative humidity at the leaf surface (%).

In addition, leaf stomatal resistance r_c (s m^{-1}) is calculated as:

$$r_c = \frac{0.625(C_s - C_i)}{A_n} \frac{\rho_a}{M_a} \frac{10^{12}}{p} \quad \text{(A9)}$$

Where ρ_a is specific mass of air (kg m^{-3}), M_a is molecular mass of dry air (g mol^{-1}), and p is atmosphere pressure (hPa).

The calculation of latent heat flux (*LE*) is as follows:

$$LE = \lambda \frac{(q_i - q_a)}{r_a + r_c} \quad \text{(A10)}$$

Where λ is vaporization heat of water (J kg^{-1}), q_i is the humidity in stomata or soil pores (kg m^{-3}), q_a is the humidity above the canopy (kg m^{-3}), r_c is stomatal or soil surface resistance (s m^{-1}), r_a is aerodynamic resistance (s m^{-1}).

In the study of Bayat et al. (2019), water stress factor was calculated based on the root zone soil moisture content neglecting the distribution of root length. In this study, water stress factor considered both root length distribution and water content in root zone. We use a sigmoid formulation rather than the piecewise function by Bayat et al. (2019). The calculations are as follows:

$$WSF = \sum_{i=1}^{n} RF(i) * WSF\ (i) \quad \text{(A11)}$$

$$WSF(i) = \frac{1}{1 + e^{-100 * \theta_{sat}\left(SM(i) - \frac{\theta_f + \theta_w}{2}\right)}} \quad \text{(A12)}$$

θ_w is the soil water content at wilting point; θ_f is the soil water content at field capacity; θ_{sat} is the saturated soil water content; *WSF(i)* is the water stress factor at each soil layer; *RF(i)* is the ratio of root length in soil layer *i* and its calculation can be found in the appendix A.4; *SM(i)* is the soil moisture at each soil layer.

A.2. Governing Equations in STEMMUS

A.2.1 Soil water conservation equation

$$\frac{\partial}{\partial t}(\rho_L \theta_L + \rho_V \theta_V) = -\frac{\partial}{\partial z}(q_{Lh} + q_{LT} + q_{La} + q_{Vh} + q_{VT} + q_{Va}) - S = \rho_L \frac{\partial}{\partial z}\left[K\left(\frac{\partial h}{\partial z} + 1\right) + D_{TD}\frac{\partial T_s}{\partial z} + \frac{K}{\gamma_w}\frac{\partial P_g}{\partial z}\right] + \frac{\partial}{\partial z}\left[D_{Vh}\frac{\partial h}{\partial z} + D_{VT}\frac{\partial T_s}{\partial z} + D_{Va}\frac{\partial P_g}{\partial z}\right] - S \quad \text{(A13)}$$

where ρ_L, ρ_V (kg m^{-3}) are the density of liquid water, water vapor, respectively; q_L , q_V (m^3 m^{-3}) are the volumetric water content (liquid and water vapor, respectively); z (m) is the vertical space coordinate (positive upwards); *S* (cm s^{-1}) is the sink term for the root water extraction. *K* (m s^{-1}) is hydraulic conductivity; *h* (cm) is the pressure head; T_s (°C) is the soil temperature; and P_g (Pa) is the mixed pore-air pressure. γ_w (kg m^{-2} s^{-2}) is the specific weight of water. D_{TD} (kg m^{-1} s^{-1} °C^{-1}) is the transport coefficient for adsorbed liquid flow due to temperature gradient; D_{Vh} (kg m^{-2} s^{-1}) is the isothermal vapor conductivity; and D_{VT} (kg m^{-1} s^{-1} °C^{-1}) is the thermal vapor diffusion coefficient. D_{Va} is the advective vapor transfer coefficient (Zeng et al. 2011a,b).

q_{Lh}, q_{LT}, and q_{La}(kg m^{-2} s^{-1}) are the liquid water fluxes driven by the gradient of matric potential, temperature, and air pressure, respectively. q_{Vh}, q_{VT}, and q_{Va} (kg m^{-2} s^{-1}) are the water vapor fluxes driven by the gradient of matric potential, temperature, and air pressure, respectively.

A.2.2 Dry air conservation equation

$$\frac{\partial}{\partial t}[\varepsilon\rho_{da}(S_a + H_c S_L)] = \frac{\partial}{\partial z}\left[D_e\frac{\partial\rho_{da}}{\partial z} + \rho_{da}\frac{S_a K_g}{\mu_a}\frac{\partial P_g}{\partial z} - H_c\rho_{da}\frac{q_L}{\rho_L} + \left(\theta_a D_{Vg}\right)\frac{\partial\rho_{da}}{\partial z}\right] \quad \text{(A14)}$$

where ε is the porosity; ρ_{da} (kg m^{-3}) is the density of dry air; S_a (=1-S_L) is the degree of air saturation in the soil; S_L (=θ_L/ε) is the degree of saturation in the soil; H_c is Henry's constant; D_e (m^2 s^{-1}) is the molecular diffusivity of water vapor in soil; K_g (m^2) is the intrinsic air permeability; m_a (kg m^{-2} s^{-1}) is the air viscosity; q_L (kg m^{-2} s^{-1}) is the liquid water flux; θ_a (=θ_V) is the volumetric fraction of dry air in the soil; and D_{Vg} (m^2 s^{-1}) is the gas phase longitudinal dispersion coefficient (Zeng et al., 2011a,b).

A.2.3 Energy balance equation

$$\frac{\partial}{\partial t}[(\rho_s\theta_s C_s + \rho_L\theta_L C_L + \rho_V\theta_V C_V + \rho_{da}\theta_a C_a)(T_s - T_r) + \rho_V\theta_V L_0] - \rho_L W\frac{\partial\theta_L}{\partial t} = \frac{\partial}{\partial z}\left(\lambda_{eff}\frac{\partial T}{\partial z}\right) - \frac{\partial}{\partial z}[q_L C_L(T_s - T_r) + q_V(L_0 + C_V(T_s - T_r)) + q_a C_a(T_s - T_r)] - C_L S(T_s - T_r) \quad \text{(A15)}$$

where C_s, C_L, C_V, C_a (J kg^{-1} °C^{-1}) are the specific heat capacities of solids, liquid, water vapor, and dry air, respectively; ρ_s(kg m^{-3}), ρ_L (kg m^{-3}), ρ_V (kg m^{-3}), and ρ_{da} (kg m^{-3}) are the density of solids, liquid water, water vapor, and dry air, respectively; θ_s is the volumetric fraction of solids in the soil; θ_L, θ_V, and θ_a are the volumetric fraction of liquid water, water vapor, and dry air, respectively; T_r (°C) is the reference temperature; L_0 (J kg^{-1}) is the latent heat of vaporization of water at temperature T_r; W (J kg^{-1}) is the differential heat of wetting (the amount of heat released when a small amount of free water is added to the soil matrix); and λ_{eff} (W m^{-1} °C^{-1}) is the effective thermal conductivity of the soil; q_L, q_V, and q_a (kg m^{-2} s^{-1}) are the liquid, vapor water and dry air flux.

A.3. Dynamic Root Growth Modelling

A.3.1. Root front growth

The depth of the root front is firstly initialized either with the sowing depth for sown crops or with an initial value for transplanted crops or perennial crops. The root front growth stops when it reached certain depth of soil or a physical/chemical obstacle preventing root growth, but also stops when the phenological stopping stage has been reached.

$$\Delta Z = \begin{cases} 0 & T_{air} < T_{min} \\ (T_{air} - T_{min}) * RGR & T_{min} < T_{air} < T_{max} \\ (T_{max} - T_{min}) * RGR & T_{max} < T_{air} \end{cases} \quad \text{(A16)}$$

$$D_Z(t) = D_Z(t-1) + \Delta Z \quad \text{(A17)}$$

where ΔZ is root front growth at *t*-th time step; D_Z (cm) is root zone depth; T_{air} (^{0}C) is air temperature; T_{min} (^{0}C) is the minimum temperature for root growth; T_{max} (^{0}C) is the maximum temperature for root growth; *RGR* (cm ^{0}C^{-1} day^{-1}) is the root growth rate of root front.

A.3.2. Root length growth

In this study, the root distribution in the root zone was realized via simulating the root length growth in each soil layer.

$$\Delta Rl\_tot = \frac{A_n * fr_{root}}{R_C * R_D * \pi * r_{root}^2} \quad \text{(A18)}$$

fr_{root} is the allocation fraction of net assimilation to root, and fr_{root} is assumed as a function of leaf area index (LAI) and root zone water content. A_n is the net assimilation rate (μmol m^{-2} s^{-1}). R_C is ratio of carbon to dry organic matter in root, R_D is root density (g m^{-3}), and r_{root} is radius of the root, and ΔRl_tot (m m^{-3}) is total root length growth.

The limiting factors for allocation are preliminarily computed and they account for root zone soil moisture availability A_W, and light availability A_L.

$$A_W = max[0.1, \quad min(1, \quad WSF)] \quad \text{(A19)}$$

where WSF is the averaged soil moisture stress factor in the root zone.

$$A_L = max[0.1, \quad e^{-K_e\, LAI}] \quad \text{(A20)}$$

where $K_e = 0.15$ is a constant light extinction coefficient.

$$fr_{root} = max\left[r_{min}, \quad r_0 \frac{3A_L}{A_L + 2A_W}\right] \quad \text{(A21)}$$

where $r_{min}(= 0.15)$ is the minimum allocation coefficient to fine roots, and r_0 is a coefficient that indicates the theoretically unstressed allocation to fine roots.

$$\Delta Rl(i) = \Delta Rl\_tot * RF(i) \quad \text{(A22)}$$

where $RF(i)$ is the allocation fraction of root growth length in layer *i*, $\Delta Rl(i)$ is the root growth length in layer *i*.

For *i* = 1 to *n-1* (*i* = 1 means the top soil layer):

$$Rl_i^t = Rl_i^{t-1} + \Delta Rl(i) \quad \text{(A23)}$$

For *i* = *n*:

$$Rl_i^t = Rl_i^{t-1} + \Delta Rl(i) + Rl_{front} \quad \text{(A24)}$$

where Rl_i^t and Rl_i^{t-1} is the root length of layer *i* at time step *t* and time step *t-1*.

$$RF(i) = \frac{Rl(i)}{Rl_T} \quad \text{(A25)}$$

where Rl_T is the total root length in root zone, $Rl(i)$ is the root length in soil layer *i*.

At the root front, the density is imposed and estimated by the parameter L_{v_front} and the growth in root length depends directly on the root front growth rate ΔZ:

$$Rl_{front} = L_{v\_front} * \Delta Z \quad \text{(A26)}$$

A.4. Root water uptake

The equation to calculate root water uptake and transpiration was as follows:

$$\sum_{i=1}^{n} \frac{\psi_{s,i} - \psi_l}{r_{s,i} + r_{r,i} + r_{x,i}} = \frac{0.622}{P} \frac{\rho_{da}}{\rho_V} \left(\frac{e_l - e_a}{r_c + r_a} \right) = T \quad \text{(A27)}$$

where $\psi_{s,i}$ is soil water potential of layer *i* (pressure head, unit: m), ψ_l is leaf water potential (m), $r_{s,i}$ is the soil hydraulic resistance (s m^{-1}), $r_{r,i}$ is the root resistance to water flow radially across the roots (s m^{-1}), and $r_{x,i}$ is the plant axial resistance to flow from the soil to the leaves (s m^{-1}). e_l and e_a are vapor pressure of leaf and the atmosphere (hPa), respectively, and r_a and r_c are aerodynamic resistance and canopy resistance (s m^{-1}), respectively. ρ_{da} is the density of dry air (kg m^{-3}). ρ_V is the density of water vapor. *P* is the atmospheric pressure (Pa). 0.622 is the ratio of the molar mass of water to air.

$\psi_{s,i}$ is described as a function of soil moisture by Van Genuchten (1980), and the relevant parameters were shown in Table B.1.

The r_s is calculated by Reid and Huck (1990) as:

$$r_s = \frac{1}{B \cdot K \cdot L_v \cdot \Delta d} \quad \text{(A28)}$$

where *B* is the root length activity factor, *K* is hydraulic conductivity of soil (m s^{-1}), L_v is root length density (m m^{-3}), and Δd is the thickness of the soil layer (m). *B* is calculated as:

$$B = \frac{2\pi}{ln\left[(\pi R_D)^{-1/2} / r_{root}\right]} \quad \text{(A29)}$$

where r_{root} is root radius (m).

The r_r is estimated as (Reid and Huck, 1990):

$$r_r = \frac{P_r(\theta_{sat}/\theta)}{L_v \Delta d} \quad \text{(A30)}$$

where P_r is root radial resistivity (s m^{-1}).

The xylem resistance r_x is estimated by Klepper et al. (1983):

$$r_x = \frac{P_a Z_{mid}}{0.5 f L_v} \quad \text{(A31)}$$

where P_a is root axial resistivity (s m^{-3}), Z_{mid} is the depth of the midpoint of soil layer, and f is a fraction defined for a specific depth as the number of roots which connect directly to the stem base to total roots crossing a horizontal plane at that depth. We can consider it equal to 0.22 based on Klepper et al. (1983).

The updated root water uptake term is:

$$S_i = \frac{\psi_{s,i} - \psi_l}{r_{s,i} + r_{r,i} + r_{x,i}} \quad \text{(A32)}$$

Different from other studies which need to calculate the compensatory water uptake and hydraulic redistribution after calculating the standard water uptake of each soil layer, the sink term in this study is calculated by a physically-based model which contain the effect of root resistance and soil hydraulic resistance rather than only considering the root fraction, so the compensatory water uptake and hydraulic redistribution have been considered when calculating the sink term.

Appendix B.

Table B.1 List of parameters and values used in this study (All the parameters were classified as Air, Canopy, Root and Soil).

Symbol	Description	Unit	Value	
Aerodynamic			Maize	Grass
aPAR	Absorbed photosynthetically active radiation	µmol m^{-2} s^{-1}		
e_a	Air vapor pressure	Pa		
e_l	Vapor pressure of leaf	hPa		
P	Air pressure	Pa		
q_a	Humidity above the canopy	kg m^{-3}		
q_l	Humidity in stomata	kg m^{-3}		
r_a	Aerodynamic resistance	s m^{-1}		
RH	Relative humidity	%		
R_{li}	Incoming longwave radiation	W m^{-2}		
R_{in}	Incoming shortwave radiation	W m^{-2}		
R_n	Net radiation	W m^{-2}		
T_{air}	Air temperature	^{0}C		
u	Wind speed	m s^{-1}		
VPD	Vapor pressure deficit	hPa		
Canopy				
A_n	Net assimilation rate	µmol m^{-2} s^{-1}		
C_a	CO_2 concentration in the boundary layer	µmol m^{-3}		
C_{ab}	Leaf chlorophyll content	µg cm^{-2}	80	0.374-50.45
C_{ca}	Leaf Carotenoid content	µg cm^{-2}	20	0.25*C_{ab}
C_w	Leaf water content	g cm^{-2}	0.009	.0.02
C_{dm}	Leaf dry matter content	g cm^{-2}	0.012	0.015
C_s	Senescent material content		0	0
DOY	Day of Year	d		
ET	Evapotranspiration	mm day^{-1}		
GPP	Gross primary production	g C m^{-2} day^{-1}		
h_c	Canopy height	m	0-1.95	0.55
H	Sensible heat flux	W m^{-2}		
J	Electron transport rate	µmol m^{-2} s^{-1}		

K_e	Light extinction coefficient		0.15	0.15
k_p	A pseudo-first-order rate constant for PEP carboxylase			
LAI	Leaf area index	$m^2\ m^{-2}$	0-4.39	0.745-2.03
LIDF	Leaf inclination distribution function		-1, 0	0.08, -0.15
LE	Latent heat flux	$W\ m^{-2}$		
LE_c	Latent heat flux of canopy	$W\ m^{-2}$		
m	Ball-Berry stomatal conductance parameter		4	10
NEE	Net ecosystem exchange	$g\ C\ m^{-2}\ day^{-1}$		
p_i	Intercellular CO_2 partial pressure	Pa		
r_c	Canopy resistance	$s\ m^{-1}$		
Re	Ecosystem respiration	$g\ C\ m^{-2}\ day^{-1}$		
T	Transpiration	$mm\ day^{-1}$		
T_c	Vegetation temperature	^0C		
T_{ch}	Leaf temperature (shaded leaves)	^0C		
T_{cu}	Leaf temperature (sunlit leaves)	^0C		
$uWUE_p$	Potential water use efficiency	$g\ C\ hPa^{0.5}/kg\ H_2O$		
uWUE	Water use efficiency	$g\ C\ hPa^{0.5}/kg\ H_2O$		
V_{cmax}	Maximum carboxylation rate	$\mu mol\ m^{-2}\ s^{-1}$	50	10.7-100.3
ψ_l	Leaf water potential	m		
Root				
A_W	Root zone soil moisture availability			
A_L	Light availability			
B	Root length activity factor			
D_Z	Root zone depth	cm		
f	A fraction defined for a specific depth as the number of roots which connect directly to the stem base to total roots crossing a horizontal plane at that depth		0.22	0.22
fr_{root}	Allocation fraction of net assimilation to root			
P_a	Root axial resistivity	$s\ m^{-3}$	$0.65*10^{12}$	$2*10^{12}$
P_r	Root radial resistivity	$s\ m^{-1}$	$1*10^{10}$	$1.2*10^{11}$
RF(i)	The allocation fraction of root growth length in layer *i*			

Rl_T	Total root length in root zone	m m^{-2}		
Rl_i^t	Root length of layer *i* at time step *t*	m m^{-2}		
Rl_i^{t-1}	Root length of layer *i* at time step *t-1*	m m^{-2}		
Rl(i)	Root length in soil layer *i*	m m^{-2}		
Rl_{front}	Growth at the root front			
RGR	Root growth rate of front	cm ^{0}C day^{-1}	0.096	0.072
R_D	Root density	g m^{-3}	250000	250000
L_v	Root length density	m m^{-3}		
L_{v_front}	Root density at the root front	m m^{-3}	1000	150
r_{min}	The minimum allocation coefficient to fine roots		0.15	0.15
r_0	Coefficient of theoretically unstressed allocation to fine roots		0.3	0.3
r_{root}	Radius of the root	m	$0.15*10^{-3}$	$1.5*10^{-3}$
$r_{x,i}$	Plant axial resistance to flow from the soil to the leaves	s		
$r_{r,i}$	Resistance to water flow radially across the roots	s		
$r_{s,i}$	Soil hydraulic resistance	s		
R_C	Ratio of carbon to dry organic matter in root	kg kg^{-1}	0.488	0.488
RWU	Root water uptake	m s^{-1}		
RF(i)	The ratio of root length in soil layer *i*			
T_{min}	Minimum temperature of root growth	^{0}C	10	0
T_{max}	Maximum temperature of root growth	^{0}C	40	40
$\triangle Z$	Root front growth at *t*-th step	cm		
$\triangle Rl\_tot$	Total root length growth	m		
$\triangle Rl(i)$	The root growth length in layer *i*	m		
Soil				
C_s	Specific heat capacities of solids	J kg^{-1} $°C^{-1}$		
C_L	Specific heat capacities of liquid	J kg^{-1} $°C^{-1}$	$4.186*10^3$	$4.186*10^3$
C_V	Specific heat capacities of water vapor	J kg^{-1} $°C^{-1}$	$1.870*10^3$	$1.870*10^3$
C_a	Specific heat capacities of dry air	J kg^{-1} $°C^{-1}$	$1.255*10^{-3}$	$1.255*10^{-3}$
D_{TD}	Transport coefficient for absorbed liquid flow due to temperature gradient	kg m^{-1} s^{-1} $°C^{-1}$		
D_{Vh}	Isothermal vapor conductivity	kg m^{-2} s^{-1}		

D_{VT}	Thermal vapor diffusion coefficient	kg m^{-1} s^{-1} °C^{-1}		
D_{Va}	Advective vapor transfer coefficient	kg m^{-2} s^{-1}		
D_{Vg}	Gas phase longitudinal dispersion coefficient	m^2 s^{-1}		
D_e	Molecular diffusivity of water vapor in soil	m^2 s^{-1}		
E	Soil evaporation	mm		
G	Soil heat flux	W m^{-2}		
h	Soil matric potential	cm		
H_c	Henry's constant		0.02	0.02
K	Hydraulic conductivity	m s^{-1}		
K_g	Intrinsic air permeability	m^2		
K_s	Saturation hydraulic conductivity	cm day^{-1}	18	10
LE_s	Latent heat flux of soil	W m^{-2}		
L_0	Latent heat of vaporization of water temperature T_r	J kg^{-1}	2497909	2497909
m_a	Air viscosity	kg m^{-1} s^{-1}	$1.846*10^{-5}$	$1.846*10^{-5}$
n	Soil-dependent parameter		1.41	1.50
P_g	Mixed pore-air pressure	Pa		
q_L	Liquid water flux	kg m^{-2} s^{-1}		
q_{Lh}	Liquid water flux driven by the gradient of matric potential	kg m^{-2} s^{-1}		
q_{LT}	Liquid water flux driven by the gradient of temperature	kg m^{-2} s^{-1}		
q_{La}	Liquid water flux driven by the gradient of air pressure	kg m^{-2} s^{-1}		
q_V	Water vapor flux	kg m^{-2} s^{-1}		
q_{Vh}	Water vapor flux driven by the gradient of matric potential	kg m^{-2} s^{-1}		
q_{VT}	Water vapor flux driven by the gradient of temperature	kg m^{-2} s^{-1}		
q_{Va}	Water vapor flux driven by the gradient of air pressure	kg m^{-2} s^{-1}		
q_a	Dry air flux	kg m^{-2} s^{-1}		
S	Sink term for the root water extraction	cm s^{-1}		
S_a	Degree of air saturation in the soil			
S_L	Degree of saturation in the soil			
$SM(i)$	The soil moisture at a specific soil layer	m^3 m^{-3}		
T_s	Soil temperature	^{0}C		
T_{s0}	Soil surface temperature	^{0}C		

T_r	Reference temperature	°C	20	20
W	Differential heat of wetting	J kg^{-1}	$1.001*10^3$	$1.001*10^3$
WSF	Total water stress factor			
$WSF(i)$	Water stress factor at a specific soil layer			
Z_{mid}	The depth of the midpoint of soil layer	m		
$\triangle d$	Thickness of the soil layer	m		
α	Soil-dependent parameter	m^{-1}	0.45	0.166
θ_{sat}	Saturated water content	m^3 m^{-3}	0.42	0.38
θ_f	Field capacity	m^3 m^{-3}	0.272	0.24
θ_w	Wilting point	m^3 m^{-3}	0.10	0.03
θ_r	Residual water content	m^3 m^{-3}	0.0875	0.0008
θ	Volumetric soil water content	m^3 m^{-3}		
θ_L	Volumetric moisture content	m^3 m^{-3}		
θ_V	Volumetric vapor content	m^3 m^{-3}		
θ_s	Volumetric fraction of solids in the soil	m^3 m^{-3}		
θ_a	Volumetric fraction of dry air in the soil	m^3 m^{-3}		
$\psi_{s,i}$	Soil water potential of layer *i*	m		
ψ_{soil}	Soil water potential	m		
λ_{eff}	Effective thermal conductivity of the soil	W m^{-1} $°C^{-1}$		
γ_w	Specific weight of water	kg m^{-2} s^{-2}		
ρ_{da}	Density of dry air	kg m^{-3}		
ρ_V	Density of vapor	kg m^{-3}		
ρ_L	Density of liquid water	kg m^{-3}	1	1
ρ_s	Density of solids	kg m^{-3}		
ε	Soil porosity	m^3 m^{-3}	0.50	0.50

References

Amato, M. and Ritchie, J.T.: Spatial distribution of roots and water uptake of maize (Zea mays L.) as affected by soil structure, Crop Sci., 42, 773-780, https://doi.org/10.2135/cropsci2002.7730, 2002.

Amenu, G. and Kumar, P.: A model for hydraulic redistribution incorporating coupled soil-root moisture transport, Hydrol. Earth Syst. Sci., 4, 3719-3769, https://doi.org/10.5194/hessd-4-3719-2007, 2007.

Aston, M. and Lawlor, D.W.: The relationship between transpiration, root water uptake, and leaf water potential, J. Exp. Bot., 30, 169-181, https://doi.org/10.1093/jxb/30.1.169, 1979.

Bayat, B., Van der Tol, C., and Verhoef, W.: Integrating satellite optical and thermal infrared observations for improving daily ecosystem functioning estimations during a drought episode, Remote Sens. Environ., 209, 375-394, https://doi.org/10.1016/j.rse.2018.02.027, 2018.

Bayat, B., Van der Tol, C., Yang, P., and Verhoef, W.: Extending the SCOPE model to combine optical reflectance and soil moisture observations for remote sensing of ecosystem functioning under water stress conditions, Remote Sens. Environ., 221, 286-301, https://doi.org/10.1016/j.rse.2018.11.021, 2019.

Beaudoin, N., Mary, B., Launay, M., and Brisson, N.: Conceptual basis, formalisations and parameterization of the STICS crop model, Quae, 2009.

Bingham, I.J. and Wu, L.: Simulation of wheat growth using the 3D root architecture model SPACSYS: validation and sensitivity analysis, Eur. J. Agron., 34, 181-189, https://doi.org/10.1016/j.eja.2011.01.003, 2011.

Caldwell, M.M., Dawson, T.E., and Richards, J.H.: Hydraulic lift: consequences of water efflux from the roots of plants, Oecologia, 113, 151-161, https://doi.org/10.1007/s004420050363, 1998.

Camargo, G. and Kemanian, A.: Six crop models differ in their simulation of water uptake, Agric. For. Meteorol., 220, 116-129, https://doi.org/10.1016/j.agrformet.2016.01.013, 2016.

Chassot, A., Stamp, P., and Richner, W.: Root distribution and morphology of maize seedlings as affected by tillage and fertilizer placement, Plant Soil, 231, 123-135, https://doi.org/10.1023/A:1010335229111, 2001.

Collatz G J, Ball J T, Grivet C et al. Physiological and environmental regulation of stomatal conductance, photosynthesis and transpiration, Agric. For. Meteorol. 54(2/3/4): 107-136, https://doi.org/10.1016/0168-1923(91)90002-8, 1991

Collatz G J, Ribas-Carbo M, Berry J A.: Coupled photosynthesis-stomatal conductance model for leaves of C4 plants, Australian Journal of Plant Physiology, 19: 519-538, 1992

Couvreur, V., Vanderborght, J., and Javaux, M.: A simple three-dimensional macroscopic root water uptake model based on the hydraulic architecture approach, Hydrol. Earth Syst. Sci., 16, 2957-2971, https://doi.org/10.5194/hess-16-2957-2012, 2012.

De Kauwe, M.G., Medlyn, B.E., Ukkola, A.M., Mu, M., Sabot, M.E., Pitman, A.J., Meir, P., Cernusak, L., Rifai, S.W., Choat, B., Tissue, D.T., Blackman, C.J., Li, X., Roderick, M. and Briggs, P.R.: Identifying areas at risk of drought-induced tree mortality across SouthEastern Australia. Glob. Change Biol., https://doi.org/10.1111/gcb.15215, 2020.

De Kauwe, M.G., Zhou, S.X., Medlyn, B.E., Pitman, A.J., Wang, Y.P., Duursma, R.A., and Prentice I.C.: Do land surface models need to include differential plant species responses to drought? examining model predictions across a mesic-xeric gradient in Europe, BIOGEOENCES, 2015,12(24), 7503-7518, https://doi.org/10.5194/bg-12-7503-2015, 2015.

Deng, Z., H. Guan, J. Hutson, M. A. Forster, Y. Wang, and C. T. Simmons.: A vegetation focused soil-plant-atmospheric continuum model to study hydrodynamic soil-plant water relations, Water Resour. Res., 53, 4965– 4983, https://doi.org/10.1002/2017WR020467, 2017.

Elfving, D. C., KAUFMANN, M. R., and HALL, A. E.: Interpreting leaf water potential measurements with a model of the soil-plant-atmosphere continuum, Physiol. Plant., 27(2), 161-168, https://doi.org/10.1111/j.1399-3054.1972.tb03594.x, 1972.

Eller, C. B., Rowland, L., Mencuccini, M., Rosas, T., Williams, K., Harper, A., Medlyn, B., Wagner, Y., Klein, T, Teodoro, G., Oliveira, R., Matos, I., Rosado, B. H. P., Fuchs, K., Wohlfahrt, G., Montagnani, L., Meir, P., Sitch, S., Cox, P.: Stomatal optimization based on xylem hydraulics (SOX) improves land surface model simulation of vegetation responses to climate, New Phytol., 226. https://doi.org/10.1111/nph.16419, 2020.

Espeleta, J., West, J., and Donovan, L.: Species-specific patterns of hydraulic lift in co-occurring adult trees and grasses in a sandhill community, Oecologia, 138, 341-349, https://doi.org/10.1007/s00442-004-1539-x, 2004.

Fan, X., Hu, H., Huang, G., Huang, F., Li, Y., and Palta, J.: Soil inoculation with Burkholderia sp. LD-11 has positive effect on water-use efficiency in inbred lines of maize, Plant and Soil 390, 337-349, https://doi.org/10.1007/s11104-015-2410-z, 2015.

Farquhar, G.D., von Caemmerer, S., and Berry, J.A.: A biochemical model of photosynthetic CO_2 assimilation in leaves of C3 species, Planta, 149, 78–90, https://doi.org/10.1007/bf00386231, 1980.

Fu, C., Wang, G., Goulden, M.L., Scott, R.L., Bible, K., and G Cardon, Z.: Combined measurement and modelling of the hydrological impact of hydraulic redistribution using CLM4. 5 at eight AmeriFlux sites, Hydrol. Earth Syst. Sci., 20, https://doi.org/10.5194/hess-2016-24-rc1, 2016.

Guo, Y.: Simulation of water transport in the soil-plant-atmosphere system, https://doi.org/10.31274/rtd-180813-9473, 1992.

Jarvis, N.: Simple physics-based models of compensatory plant water uptake: Concepts and eco-hydrological consequences, Hydrol. Earth Syst. Sci., 15, 3431-3446, https://doi.org/10.5194/hess-15-3431-2011, 2011.

Jones, J.W., Hoogenboom, G., Porter, C.H., Boote, K.J., Batchelor, W.D., Hunt, L., Wilkens, P.W., Singh, U., Gijsman, A.J., and Ritchie, J.T.: The DSSAT cropping system model, Eur. J. Agron., 18, 235-265, https://doi.org/10.1016/s1161-0301(02)00107-7, 2003.

Keating, B.A., Carberry, P.S., Hammer, G.L., Probert, M.E., Robertson, M.J., Holzworth, D., Huth, N.I., Hargreaves, J.N., Meinke, H., and Hochman, Z.: An overview of APSIM, a model designed for farming systems simulation, Eur. J. Agron., 18, 267-288, https://doi.org/10.1016/s1161-0301(02)00108-9, 2003.

Kennedy, D., Swenson, S., Oleson, K.W., Lawrence, D.M., Fisher, R. A., da Costa, A., and Gentine, P.: Implementing plant hydraulics in the community land model, version 5, J. Adv. Model. Earth Syst., https://doi.org/10.1029/2018MS001500, 2019.

Klepper, B., Rickman, R.W., and Taylor, H.M.: Farm management and the function of field crop root systems, Agric. Water Manage., 7, 115–141, https://doi.org/10.1016/0378-3774(83)90078-1, 1983.

Krinner, G., N. Viovy, N. de Noblet-Ducoudre, J. Ogee, J. Polcher, P. Friedlingstein, P. Ciais, S. Sitch, and I. C. Prentice.: A dynamic global vegetation model for studies of the coupled atmosphere-biosphere system, Glob. Biogeochem. Cycle, 19 (GB1015), doi:10.1029/2003GB002199, 2005.

Lawrence, D., Fisher, R., Koven, C., Oleson, K., Swenson, S., Vertenstein, M.: Technical Description of version 5.0 of the Community LandModel (CLM), 2020.

Leitner, D., Klepsch, S., Bodner, G., and Schnepf, A.: A dynamic root system growth model based on L-Systems, Plant Soil, 332, 177-192, https://doi.org/10.1007/s11104-010-0284-7, 2010.

Mackay, D.S., Savoy, P. R., Grossiord, C., Tai, X., Oleban, J., Wang, D., McDowell, N., Adams, H., Sperry, J. S.: Conifers depend on established roots during drought: results from a coupled model of carbon allocation and hydraulics, New Phytol., 225(2), 679-692, https://doi.org/10.1111/nph.16043, 2019.

Martineau, E., Domec, J.-C., Bosc, A., Denoroy, P., Fandino, V.r.A., Lavres Jr, J., and Jordan-Meille, L.: The effects of potassium nutrition on water use in field-grown maize (Zea mays L.), Environ. Exp. Bot., 134, 62-71, https://doi.org/10.1016/j.envexpbot.2016.11.004, 2017.

Medlyn, B.E., Kauwe, M.G.D., and Duursma, R.A.: New developments in the effort to model ecosystems under water stress, New Phytol., 212(1), 5-7, https://doi.org/10.1111/nph.14082, 2016.

Mcdowell, N.G., Brodribb, T.J., and Nardini, A.: Hydraulics in the 21st century, New Phytol., 224(2), https://doi.org/10.1111/nph.16151, 2019.

Mohammed, G.H., Colombo, R., Middleton, E.M., Rascher, U., Van der Tol, C., Nedbal, L., Goulas Y., Perez-Priego, O., Damm A., Meroni M., Joiner J., Cogliati S., Verhoef W., Malenovsky Z., Gastellu-Etchegorry J., Miller, J., Guanter, L., Moreno, J., Berry, J., Frankenberg, C., Zarco-Tejada, P.J.: Remote sensing of solar-induced chlorophyll fluorescence (SIF) in vegetation: 50 years of progress. Remote Sens. Environ., 231, https://doi.org/10.1016/j.rse.2019.04.030, 2019.

Ning, P., Li, S., White, P.J., and Li, C.: Maize varieties released in different eras have similar root length density distributions in the soil, which are negatively correlated with local concentrations of soil mineral nitrogen, PLOS one, 10, e0121892, https://doi.org/10.1371/journal.pone.0121892, 2015.

Niu, G., Fang, Y., Chang, L., Jin, J., Yuan, H., and Zeng, X.: Enhancing the Noah-MP ecosystem response to droughts with an explicit representation of plant water storage supplied by dynamic root water uptake, J. Adv. Model. Earth Syst., https://doi.org/10.1029/2020MS002062, 2020.

O'Toole, J.C., and Cruz, R.T.: Response of leaf water potential, stomatal resistance, and leaf rolling to water stress, Plant Physiol., 65, 428-432, https://doi.org/10.1104/pp.65.3.428, 1980.

Oikeh, S., Kling, J., Horst, W., Chude, V., and Carsky, R.: Growth and distribution of maize roots under nitrogen fertilization in plinthite soil, Field Crop. Res., 62, 1-13, https://doi.org/10.1016/s0378-4290(98)00169-5, 1999.

Peng, Y., Yu, P., Zhang, Y., Sun, G., Ning, P., Li, X., and Li, C.: Temporal and spatial dynamics in root length density of field-grown maize and NPK in the soil profile, Field Crop. Res., 131, 9-16, https://doi.org/10.1016/j.fcr.2012.03.003, 2012.

Qin, R., Stamp, P., and Richner, W.: Impact of tillage on maize rooting in a Cambisol and Luvisol in Switzerland, Soil Tillage Res., 85, 50-61, https://doi.org/10.1016/j.still.2004.12.003, 2006.

Reichstein, M., Falge, E., Baldocchi, D., Papale, D., Aubinet, M., Berbigier, P., Bernhofer, C., Buchmann, N., Gilmanov, T., and Granier, A.: On the separation of net ecosystem exchange into assimilation and ecosystem respiration: review and improved algorithm, Glob. Change Biol., 11, 1424-1439, https://doi.org/10.1111/j.1365-2486.2005.001002.x, 2005.

Reid, J.B., and Huck, M.G.: Diurnal variation of crop hydraulic resistance: a new analysis, Agron. J., 82, 827–834. https://doi.org/10.1016/0378-3774(90)90029-X, 1990.

Richards, J.H. and Caldwell, M.M.: Hydraulic lift: substantial nocturnal water transport between soil layers by Artemisia tridentata roots, Oecologia, 73, 486-489, https://doi.org/10.1007/bf00379405, 1987.

Robertson, M., Fukai, S., Hammer, G., and Ludlow, M.: Modelling root growth of grain sorghum using the CERES approach, Field Crop. Res., 33, 113-130, https://doi.org/10.1016/0378-4290(93)90097-7, 1993.

Ryel, R., Caldwell, M., Yoder, C., Or, D., and Leffler, A.: Hydraulic redistribution in a stand of Artemisia tridentata: evaluation of benefits to transpiration assessed with a simulation model, Oecologia, 130, 173-184, https://doi.org/10.1007/s004420100794, 2002.

Schroder, J., Groenwold, J., and Zaharieva, T.: Soil mineral nitrogen availability to young maize plants as related to root length density distribution and fertilizer application method, NJAS-Wagen. J. Life Sci., 44, 209-225, 1996.

Seneviratne, S.I., Corti, T., Davin, E. L., Hirschi, M., Jaeger, E., B., L., I., Orlowsky, B., and Teuling A. J.: Investigating soil moisture-climate interactions in a changing climate: a review, Earth-Sci. Rev, 99, 125–161, https://doi.org/10.1016/j.earscirev.2010.02.004, 2010.

Shan, N., Ju, W., Migliavacca, M., Martini, D., Guanter, L., and Chen, J.M., Goulas, Y., Zhang, Y.. Modeling canopy conductance and transpiration from solar-induced chlorophyll fluorescence, Agric. For. Meteorol., 268, 189-201, https://doi.org/10.1016/j.agrformet.2019.01.031, 2019.

Stöckle, C.O., Donatelli, M., and Nelson, R.: CropSyst, a cropping systems simulation model, Eur. J. Agron., 18, 289-307, https://doi.org/10.1016/s1161-0301(02)00109-0, 2003.

Sun, Y., Fu, R., Dickinson, R., Joiner, J., Frankenberg, C.,Gu, L., Xia, Y., Fernando, N.: Drought onset mechanisms revealed by satellite solar-induced chlorophyll fluorescence: insights from two contrasting extreme events, J. Geophys. Res.-Biogeosci., 120(11), 2427-2440, https://doi.org/10.1002/2015JG003150, 2016.

Supit, I., Hooijer, A., and Van Diepen, C.: System description of the WOFOST 6.0 crop simulation model implemented in CGMS, vol. 1: Theory and Algorithms, Joint Research Centre, Commission of the European Communities, EUR 15956, 146, 1994.

Van Dam, J.C.: Field-Scale Water Flow and Solute Transport. SWAP ModelConcepts, Parameter Estimation and Case Studies, Wageningen University, Wageningen, The Netherlands, pp. 167, 2000.

Van der Tol, C., Verhoef, W., Timmermans, J., Verhoef, A., and Su, Z.: An integrated model of soil-canopy spectral radiances, photosynthesis, fluorescence, temperature and energy balance, Biogeosciences, 6, 3109-3129, https://doi.org/10.5194/bg-6-3109-2009, 2009.

Van der Tol, C., Berry, J., Campbell, P., Rascher, U.: Models of fluorescence and photosynthesis for interpreting measurements of solar-induced chlorophyll fluorescence, J. Geophys. Res.-Biogeosci., 119, 2312–2327, doi:10.1002/2014JG002713, 2014.

Van Genuchten, M.T.: A closed-form equation for predicting the hydraulic conductivity of unsaturated soils, Soil Sci. Soc. Am. J., 44, 892–898, https://doi.org/10.2136/sssaj1980.03615995004400050002x, 1980.

Wang, E. and Smith, C.J.: Modelling the growth and water uptake function of plant root systems: a review, Aust. J. Agr. Res., 55, 501-523, https://doi.org/10.1071/ar03201, 2004.

Wang, Y., Cai, HJ., Zeng, YJ., Su, Z., and Yu, LY.: Data underlying the research on Seasonal and interannual variation in evapotranspiration, energy flux, and Bowen ratio over a dry semi-humid cropland in Northwest China, 4TU. Centre for Research Data. Dataset, https://doi.org/10.4121/uuid:aa0ed483-701e-4ba0-b7b0-674695f5f7a7, 2019.

Wang, Y., Cai, HJ, Yu, LY., Peng XB., Xu JT., and Wang XW.: Evapotranspiration partitioning and crop coefficient of maize in dry semi-humid climate regime, Agric. Water Manage[preprint], 236, https://doi.org/10.1016/j.agwat.2020.106164, 2020a.

Wang, Y., Zeng, YJ., Yu, LY, Yang P., Van der Tol C., Su, Z., and Cai, HJ.: Integrated Modelling of Photosynthesis and Transfer of Energy, Mass and Momentum (STEMMUS-SCOPE v1.0), Zenodo, https://doi.org/10.5281/zenodo.3839092, 2020b.

Wiesler, F. and Horst, W.: Root growth and nitrate utilization of maize cultivars under field conditions, Plant Soil, 163, 267-277, https://doi.org/10.1007/bf00007976, 1994.

Williams, J., Jones, C., Kiniry, J., and Spanel, D.A.: The EPIC crop growth model. Transactions of the ASAE, 32, 497-0511, https://doi.org/10.13031/2013.31032, 1989.

Williams, J.R., Gerik, T., Francis, L., Greiner, J., Magre, M., Meinardus, A., Steglich, E., and Taylor, R.: EPIC – Environmental Policy Integrated Climate Model – UsersManual version 0810, Blackland Research and Extension Center – Texas A&MAgriLife, Temple, TX, 2014.

Williams, M., Rastetter, E. B., Fernandes, D.N., Goulden, M. L., Wofsy, S.C., Shaver G.R., Melillo J.M., Munger, J.W., Fan, S.M., and Nadelhoffer, K. J.: Modelling the soil-plant-atmosphere continuum in a Quercus-Acer stand at Harvard Forest: the regulation of stomatal conductance by light, nitrogen and soil/plant hydraulic properties, Plant Cell Environ., 19(8), 911-927, https://doi.org/ 10.1111/j.1365-3040.1996.tb00456.x, 1996.

Wu, L., McGechan, M., Watson, C., and Baddeley, J.: Developing existing plant root system architecture models to meet future agricultural challenges, Adv. Agron., 85, 85004-85001, https://doi.org/10.1016/s0065-2113(04)85004-1, 2005.

Xu, L. and Baldocchi, D. D.: Seasonal trends in photosynthetic parameters and stomatal conductance of blue oak (Quercus douglasii) under prolonged summer drought and high temperature, Tree Physiol., 23(13), 865-877, https://doi.org/10.1093/treephys/23.13.865, 2003.

Xu, X., Medvigy, D., Powers, J.S., Becknell, J.M., and Guan, K.: Diversity in plant hydraulic traits explains seasonal and inter-annual variations of vegetation dynamics in seasonally dry tropical forests, New Phytol., 212(1), https://doi.org/10.1111/nph.14009, 2016.

Yu, L., Zeng, Y., Su, Z., Cai, H., and Zheng, Z.: The effect of different evapotranspiration methods on portraying soil water dynamics and ET partitioning in a semi-arid environment in Northwest China, Hydrol. Earth Syst. Sci., 20, 975-990, https://doi.org/10.5194/hess-20-975-2016, 2016.

Yu, L., Zeng, Y., Wen, J., and Su, Z.: Liquid-Vapor-Air Flow in the Frozen Soil, J. Geophys. Res.-Atmos., 123(14), 7393-7415, https://doi.org/10.1029/2018jd028502, 2018.

Zeng, Y., Su, Z., Wan, L., and Wen, J.: A simulation analysis of the advective effect on evaporation using a two-phase heat and mass flow model, Water Resour. Res., 47(10), W10529, https://doi.org/10.1029/2011wr010701, 2011a.

Zeng, Y., Su, Z., Wan, L., and Wen, J.: Numerical analysis of air-water-heat flow in unsaturated soil: Is it necessary to consider airflow in land surface models?, J. Geophys. Res.-Atmos., 116(D20), D20107, https://doi.org/10.1029/2011jd015835, 2011b.

Zeng, Y. and Su, Z.: STEMMUS: Simultaneous Transfer of Engery, Mass and Momentum in Unsaturated Soil, University of Twente, Faculty of Geo-Information and Earth Observation (ITC), Enschede, 2013.

Zhang, Y., Guanter, L., Joiner, J., Song, L., and Guan, K.: Spatially-explicit monitoring of crop photosynthetic capacity through space-based chlorophyll fluorescence data, Remote Sens. Environ., 210, 362-374, https://doi.org/10.1016/j.rse.2018.03.031, 2018.

Zhang, Z., Zhang, Y.G., Porcar-Castell, A., Joiner, J., Guanter, L., Yang, X., Migliavacca, M., Ju, W., Sun, Z., Chen, S., Martini, D., Zhang, Q., Li, Z., Cleverly, J., Wang, H., and Goulas, Y.: Reduction of structural impacts and distinction of photosynthetic pathways in a global estimation of GPP from space-borne solar-induced chlorophyll fluorescence, Remote Sens. Environ., 111722. https://doi.org/10.1016/j.rse.2020.111722, 2020.

Zheng, Z. and Wang, G.: Modelling the dynamic root water uptake and its hydrological impact at the Reserva Jaru site in Amazonia, J. Geophys. Res.-Biogeosci., 112, https://doi.org/10.1029/2007jg000413, 2007.

Zhou, S., Duursma, R.A., Medlyn, B.E., Kelly, J.W., and Prentice, I.C.: How should we model plant responses to drought? An analysis of stomatal and non-stomatal responses to water stress, Agric. For. Meteorol., 182, 204-214, https://doi.org/10.1016/j.agrformet.2013.05.009, 2013.

Zhou, S., Yu B., Huang Y., and Wang G.: The effect of vapor pressure deficit on water use efficiency at the subdaily time scale, Geophys. Res. Lett., 41, 5005–5013, doi:10.1002/2014GL060741, 2014.

Zhou, S., Yu, B., Zhang, Y., Huang, Y., and Wang, G.: Partitioning evapotranspiration based on the concept of underlying water use efficiency, Water Resour. Res., 52, 1160-1175, https://doi.org/10.1002/2015wr017766, 2016.

Zhu, S., Chen, H., Zhang, X., Wei, N., Shangguan, W., Yuan, H., Zhang, S., Wang, L., Zhou, L., and Dai, Y. Incorporating root hydraulic redistribution and compensatory water uptake in the Common Land Model: Effects on site level and global land modelling, J. Geophys. Res.-Atmos., 122, 7308-7322, https://doi.org/10.1002/2016jd025744, 2017.

Zhuang, J., Nakayama, K., Yu, G.-R., and Urushisaki, T.: Estimation of root water uptake of maize: an ecophysiological perspective, Field Crop. Res., 69, 201-213, https://doi.org/10.1016/s0378-4290(00)00142-8, 2001a.

Zhuang, J., Yu, G., and Nakayama, K.: Scaling of root length density of maize in the field profile, Plant Soil, 235, 135-142, https://doi.org/10.1023/A:1011972019617, 2001b.